MEASUREMENT OF ZENITH NIGHT SKY LUMINANCE IN THE CITY OF BREMEN AND SURROUNDINGS

by

Kai Pong Tong

A thesis submitted to the
Institute of Environmental Physics, University of Bremen
in partial fulfillment of the requirements for the degree of
Master of Science in Environmental Physics

Institut für Umweltphysik

Universität Bremen

August, 2012

Declaration

I declare that this thesis represents my own work, except where due acknowledgement is made, and that it has not been previously included in a thesis, dissertation or report submitted to this University or to any other institution for a degree, diploma, or other qualifications.

Kai Pong Tong
Bremen, August, 2012

Abstract

Light pollution has many adverse effects on human beings and ecology. Previously various studies found the relationship between population of city and night sky luminance. Although Bremen is the 10th largest city in terms of population in Germany, little was known about the situation of light pollution. Therefore in-situ long-term measurement is needed in order to assess the impact of light pollution of the city to the nature. In this study , two low-cost photometers were inter-compared before setting up for zenith night sky luminance measurement in the campus of the University of Bremen and in Seebergen near Lilienthal, Lower Saxony. Under clear sky, the campus, which is situated in the suburban area of Bremen, is nearly three times brighter than in Seebergen, which is in the rural area near Bremen. The cloudy sky at the campus is 13.4 times as bright as the clear sky, whereas in the rural site of Seebergen, the increase of night sky luminance under overcast sky is only 50%. In addition, the change of clear sky luminance with respect to time were found. The data was also compared with dataset acquired at 19 different sites in Europe and North America in summer 2011 and was found to be consistent with each other. With the help of this findings, the ecological impact of anthropogenic light in Bremen can be evaluated.

Acknowledgements

First of all I would like to express my gratitude to Prof. Dr. Justus Notholt, Dr. Annette Ladstätter-Weißenmayer for their supervision, guidance and support for me to start up this project here in Bremen. I would also like to thank Dr. Christopher C. M. Kyba of the Freie Universität Berlin for his invaluable suggestions and giving me the opportunity to work in the International SQM Survey.

Without the support and help from many people, this thesis would never become a reality. I would like to say thank you to Christine Weinzierl for all the technical support and providing me the measurement site in the rural area of Bremen. I also would like to thank Dr. Dorien Lolkema from RIVM, the Netherlands for the technical advices in SQM inter-comparison. My thankfulness also goes to Terry Wong, Chu Wing So and Dr. Jason Chun Sing Pun of the University of Hong Kong for inspiring me to work on this interesting topic.

I would like to thank everyone in the PHAROS Group for the amazing working environment and their encouragement. I also will never forget my fellows in the PEP program for the two years of enjoyable life here in Bremen.

I am indebted to Prof. Dr. Yaping Shao of the University of Cologne for his encouragement for me to continue my study in Germany at the toughest time of my life.

I dedicate this work to my family for their unconditional support.

Contents

1 Introduction **1**

1.1 What is Light Pollution . . . 1

1.2 Fundamentals in Sky Brightness . . . 1

1.2.1 Photometric Units used in Quantifications of Night Sky Brightness . . . 1

1.2.2 Background Sky Luminance . . . 2

1.3 Adverse Effects of Light Pollution . . . 3

1.4 Overview of Light Pollution Studies . . . 5

2 Rationale for Light Pollution Measurements and Study in Bremen **7**

2.1 Geographic and Demographic Overview of Bremen . . . 7

2.2 Extent of Knowledge about Light Pollution in Bremen . . . 8

2.3 Purpose of Night Sky Luminance Measurement . . . 8

3 Inter-Comparison of Photometers **9**

3.1 Instrumentation . . . 9

3.2 Measurement Site . . . 11

3.3 Installation of SQM-LEs and Data Acquisition . . . 12

3.4 Measurement of Attenuation of Housing Glass Window . . . 13

3.5 Data Analysis . . . 14

3.6 Results and Discussion . . . 15

4 Analysis of Dataset outside Bremen **19**

4.1 Measurement Campaign of International SQM Survey . . . 19

4.1.1 Investigation of Amplification Effect by Reflection of Clouds - Cloud coverage analysis . . . 21

4.1.2 Change of Sky Luminance during the Night - Average night sky luminance time series . . . 23

4.2 Data Analysis . . . 23

4.2.1 Preprocessing for Raw Datasets . . . 23

4.2.2 Data Reduction and Processing for Cloud Coverage Analysis and Night Time Cloud-free Time Series . . . 24

4.2.3 Error Analysis . . . 24

4.3 Results and Discussion . . . 29

4.3.1 Cloud coverage analysis . . . 29

4.3.2 Average night sky luminance time series . . . 31

5 Night Sky Monitoring in Bremen **33**
5.1 Methodology . . . 33
5.2 Results and Discussion . . . 35
5.2.1 Cloud coverage analysis . . . 35
5.2.2 Average night sky luminance time series . . . 37
5.2.3 Comparison with International SQM Servey data . . . 38

6 Conclusions **41**

A Results for selected International SQM Survey Sites **43**

B List of Data Providers of International SQM Survey **73**

List of Figures

1.1 Overview of contributions from different sources of light using modeled and experimental data 4
1.2 Equilibrium shift towards NO_2 in the presence of anthropogenic lights 5

3.1 SQM-LE night sky luminance photometer 9
3.2 Relative spectral response of SQM 10
3.3 SQM-LE in use 11
3.4 Mounting of SQM-LEs. 12
3.5 Schematic diagram of SQM-LE network setup during inter-comparison 13
3.6 Schematic diagram of calibraion box 14
3.7 An example of discrepancy between instruments under moonlight . . 15
3.8 Scatter plots for Inter-comparison of Bremen SQM-LEs 16

4.1 Map of International SQM Survey sites 22
4.2 The resulting fit for the quantization uncertainty 26
4.3 Overcast sky luminance against clear sky luminance scatter plot for selected International SQM Survey datasets 30

5.1 Setup of SQM-LE at the rural site in Seebergen, Lilienthal 34
5.2 A map showing the measurement sites in Bremen and the used SYNOP station 34
5.3 Cloud coverage analysis plot for Bremen dataset 36
5.4 Average night sky luminance time series for Bremen 37
5.5 Camparison of clear sky and overcast sky luminances in Bremen with International datasets 38

List of Tables

3.1 Geolocational data for measurement site NW1, University of Bremen 12
3.2 Results for Glass Window Attenuation Test 14

4.1 List of International SQM Survey sites 20
4.2 RMS error by luminance reading for quantization uncertainty fit . . . 25
4.3 Summary of Results for cloud coverage analysis of International SQM Survey 29

5.1 List of Bremen night sky monitoring sites 33
5.2 Results for cloud coverage analysis of Bremen dataset 35
5.3 Linear cloud amplification factors for Bremen dataset 36

Chapter 1

Introduction

1.1 What is Light Pollution

Since the existence of human beings, lighting is one of the most indispensable tools in everyday life, due to the dependence of vision to carry out various kind of works. Since the controlled use of fire by human beings, its associated production of light [9] extended the active hours of human beings beyond the daytime. As modern civilizations of the humans developed, production of anthropogenic light became much easier. As a consequence, we can use lights virtually anywhere, and whenever we want. However, not all the light emitted by devices are directed towards the places where lighting is needed.

Light pollution is defined, by the International Dark-Sky Association (IDA)[1], as

> "Any adverse effect of artificial light, including sky glow, glare, light trespass, light clutter, decreased visibility at night, and energy waste"

1.2 Fundamentals in Sky Brightness

1.2.1 Photometric Units used in Quantifications of Night Sky Brightness

Depending on the applications, astronomers use different photometric units and standards for quantifying the brightness of objects. In this study, the luminance of the night sky is quantified. Luminance (also called radiance) is defined as the

[1] `http://www.darksky.org`

radiant flux per unit area per solid angle. The luminance, L_v, can be described by the following derivative:

$$L_v = \frac{1}{cos\,\theta}\frac{dI}{dS} \tag{1.1}$$

where θ is the incidence angle to the surface, I the radiant intensity and S the surface area [29].

In astronomy, a relative logarithmic unit, called the magnitude (mag in short), is also used. One magnitude of difference is approximately equal to a difference of a factor of 2.5 in luminance. Let I_1 be the radiant intensity of one stellar object and I_2 be that of another stellar object, the difference in magnitude, Δm, can be expressed by [34]

$$\Delta m = m_1 - m_2 = -2.5\,log_{10}(\frac{I_1}{I_2}) \tag{1.2}$$

Defining the magnitude in this way, 5 magnitudes of difference is exactly equal to a factor of 100.

Zero magnitude had been historically defined by the brightness of Vega. However, it was found that Vega's brightness has some variability due to its rapid-rotating nature. Therefore, various calibration standard replacements for Vega have been proposed, including model spectra and other stars with more stable emissions [20].

1.2.2 Background Sky Luminance

The most significant cause for the complexity in light pollution measurements is that the sky itself has a background luminance, even in the absence of anthropogenic contribution. In 1998, Leinert et al. summarized the contribution of diffuse night sky brightness applicable to the sky after astronomical twilight and without contribution from moonlight, in the wavelength region between 100 nm and 200 μm [14]:

- Airglow. This arises from the excitation of oxygen and nitrogen atoms at the ionosphere. Intensity denoted by I_A.

- Zodiacal light. This comes from scattered sunlight traveling along the atmosphere, as well as thermal excitation of interplanetary particles. Intensity denoted by I_{ZL}.

- Integrated starlight. This is the integral of contribution of light from stars which are not treated individually due to low brightness. Intensity denoted by I_{ISL}.
- Diffuse galactic light. This accounts for the light emitted or diffused by the dust particles of our galaxy which is dominant at the Far-IR region of the spectrum but affects visible region too. Denoted by I_{DGL}.
- Extragalactic background light. This is the contribution by all objects outside our galaxy. Denoted by I_{EBL}.
- Incoming scattered light. This contains all the portion of brightness which is scattered into the region of observation. For a light pollution-free night sky, this may arise from the scattering of all natural light sources stated above. Denoted by I_{sca}.

The total sky brightness, I_{tot}, can then be expressed by

$$I_{tot} = (I_A + I_{ZL} + I_{ISL} + I_{DGL} + I_{EBL})exp(-\tau) + I_{sca} \tag{1.3}$$

when considering also the extinction of light by the atmosphere, with τ being the extinction coefficient, which depends on wavelength, zenith angle, height of the observer and atmospheric composition.

If the latitude of the site is larger than 40°, then the effect of aurora is also not negligible.

The contributions from these sources can be seen in Figure 1.1 [14].

In the presence of artificial light, I_{sca} varies correspondingly. This is the focus of the study at hand.

1.3 Adverse Effects of Light Pollution

There are many adverse effects associated with light pollution. The most well-known of which is on astronomical observations. Numerous research groups have tried to evaluate the negative effects of light pollution on star observations. Other effects of light pollution can be roughly classified as health effects, ecological impacts and indirect enhancement of other pollution problems.

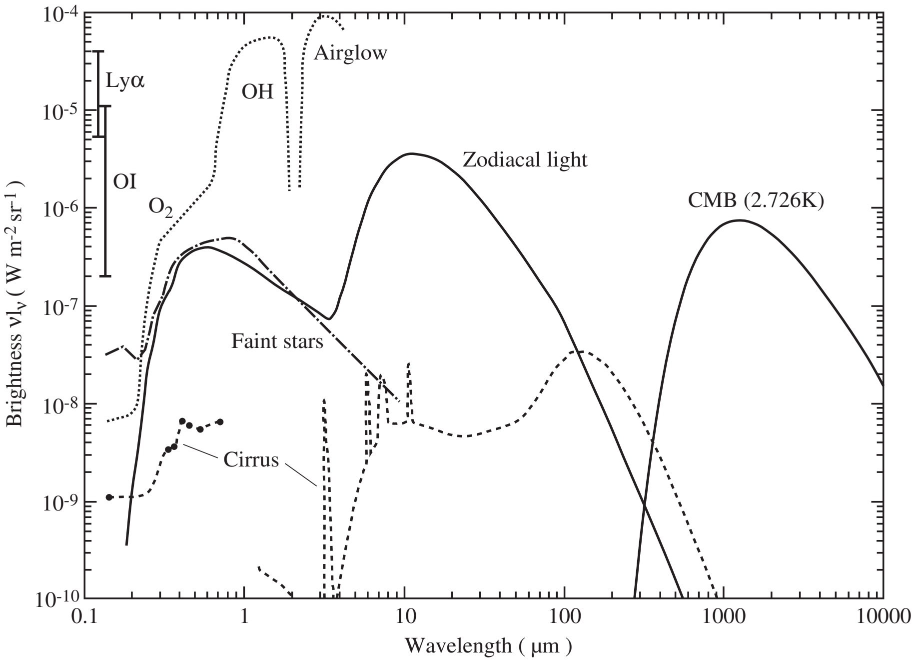

Figure 1.1: Overview of contributions from different sources of light using modeled and experimental data [14].

Effects on Human Health

It is well-known and can be shown [32] that unwanted artificial light can disrupt the circadian rhythm of human beings. Inappropriate artificial lighting can cause increased likelihood of development of depression and other psychological problems [24], and even can indirectly increase the risk of various tumors, for example breast cancer [16, 30, 21].

Impact on Ecological Systems

The responses to spectral ranges of light for different species of animals and plants vary, and there are potential hazards for inappropriate artificial lighting to ecological systems. Many animal species, for example moths, night-flying birds and sea turtles, are attracted by lamps. In some cases, this can cause disorientations and may eventually cause deaths [21, 18]. Light pollution also affects the reproduction and foraging of animals, and the growth pattern of plants can be altered.

Indirect Enhancements of Other Forms of Pollution

Since light pollution is directly related to the increase of number of photons traveling through the atmosphere, this implies that many photochemical reactions involved in air pollution can be influenced during night. For example, nitrate radicals destruction is enhanced in the presence of anthropogenic lights (refer to Figure 1.2 for example), and ozone concentration increases correspondingly [27]. One of the possible reactions is as below:

$$NO_3 + O_2 \xrightarrow{h\nu} NO_2 + O_3 \tag{1.4}$$

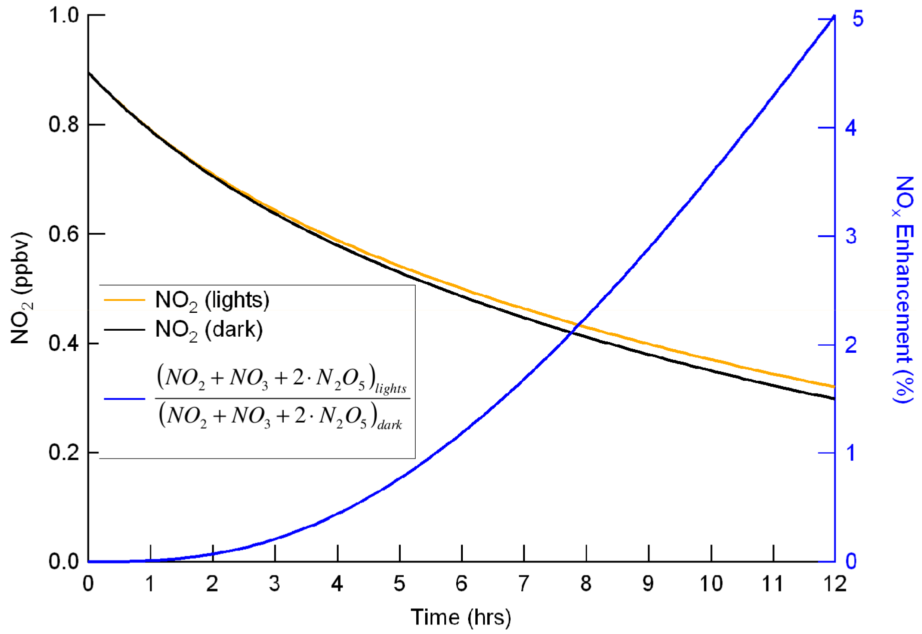

Figure 1.2: Equilibrium shift towards NO_2 in the presence of anthropogenic lights [27].

In addition, light pollution can also be used as an indicator of energy waste in lighting. Some studies exploited the measurement of light pollution by satellite as a method for estimation of energy consumption [15, 17].

1.4 Overview of Light Pollution Studies

Light pollution was first mentioned in the early 1970s, when astronomers in the USA discovered the increasing trend of night sky luminance, and sites suitable for astronomical observations became more difficult to find [22]. Before that, studies on effects of artificial light source on animal behaviors took place, some of which can be traced back to mid-1920s [23, 11, 8]. However, it was not before 1990s when more in-depth studies on the subject areas mentioned in the previous sections were conducted.

Quantitative studies of light pollution usually involve analyses of remote sensing images obtained by satellites. One of the most common choices is the Defense Meteorological Satellite Program (DMSP). Since the Operational Linescan System (OLS) on-board the DMSP satellites is capable to observe radiation in the visible light, it is suitable for large-area upwelling artificial light measurements at a wavelength band between 440nm and 940nm [3].

There are several ground-based large-scale surveys and measurement campaigns dedicated for the quantification of light pollution. The largest project of this type is the GLOBE at Night project[2]. This project requests volunteers to compare the night sky observed by naked eye with provided night sky charts for classifying the night sky brightness, or measuring the zenith night sky brightness using low-cost portable lightmeters, namely the Sky Quality Meters (SQMs) manufactured by Unihedron[3], Canada. In 2011 the project collected around 14,200 data from 115 countries. Another project with similar goal is the Buiometria Partecipativa[4] (BMP, in English Participatory Sky Quality Measurement) of Italy, which invites volunteers from the country for measuring the night sky brightness of different locations using the SQMs since 2008. This approach had also been deployed by the University of Hong Kong for the project A Survey of Light Pollution in Hong Kong [26, 25]. Some continuous measurement networks also exist, for example the Verlust der Nacht project which operates a network in Berlin[5], and the Hong Kong Night Sky Brightness Monitoring Network[6].

[2]`http://www.globeatnight.org/`
[3]`http://www.unihedron.com/`
[4]`http://www.pibinko.org/bmp2/`
[5]`http://www.verlustdernacht.de`
[6]`http://nightsky.physics.hku.hk`

Chapter 2

Rationale for Light Pollution Measurements and Study in Bremen

In 1976, Berry [1] carried out photometry of night skies in Southern Ontario and found a relationship between population and light pollution. Walker [33] also observed in 1977 a similar trend in California. Therefore, population plays an important role in the magnitude of light pollution, and knowledge of geographic and demographic situation is vital for night sky luminance studies. In this chapter, Some basics in geography and demography of the City of Bremen, as well as the status of light pollution research, will be described. These will serve as the rationale for the need of quantitative measurement for the city.

2.1 Geographic and Demographic Overview of Bremen

Bremen is a city situated in northern Germany. Built along the Weser River, it is an independent city of state of the Free Hanseatic City of Bremen. The coordinates of city is at around 53° North, 9° East, with a length of 38 km and a width of 16 km [28]. According to the data from the Federal Statistical Office of Germany[1], the city of Bremen has a population of 547,340 and an area of 325.47 km^2 as of December, 2010. It is the 10^{th} largest independent city in terms of population, and the 5^{th} largest independent city in terms of land area. Using the data above, it can be estimated that the population density is approximately 1,681.7 /km^2.

[1] http://www.statistik-portal.de/

2.2 Extent of Knowledge about Light Pollution in Bremen

Little is known about light pollution research or night sky luminance measurement conducted in or related to the city of Bremen.

One of the few information about night sky brightness of Bremen was mentioned by Hänel in the European Dark-Skies Symposium 2006, when he studied the change in upwelling light from 1993 to 2002 measured by DMSP F10 and F15 satellites in central Europe. It was noticed that the measured upwelling brightness of Bremen decreased in 2002 in comparison to that of 1993. However, no conclusion was made for the cause of the decrease [7]. In addition, Hänel also measured the sky luminance at the outskirt of Bremen[2]

Apart from that, there are only sparse night sky measurement data submitted to the Internet by individuals.

2.3 Purpose of Night Sky Luminance Measurement

Considering the high population and population density of the city, and the lack of detailed information about the night sky luminance, the potential hazards of human health and ecological impacts induced by light pollution are still unknown. In order to have a better understanding to this issue, a quantitative study in night sky luminance is necessary. Also, by long-term sky luminance measurement, the change of situation in light pollution of Bremen will be observed. Further, the results for measurements can be incorporated into international databases, which may help deepening the understanding on this subject further.

In addition to a better understanding of the issue of light pollution, a research in this field may serve as a tool for increasing public awareness. This has been successfully done by many large-scale voluntary surveys and light pollution measurement campaigns. One of these examples is the project A Survey of Light Pollution in Hong Kong [26, 25], which did not only carry out a light pollution map for Hong Kong, but also successfully increased awareness of general public towards the issue of light pollution, and in addition attracted media coverage[3].

[2]Personal communication with Andreas Hänel.
[3]For details see `http://nightsky.physics.hku.hk/reference-hong-kong-media.php`

Chapter 3

Inter-Comparison of Photometers

In order to check the consistency between the readings produced by individual photometers, an inter-comparison of the photometers over a sufficiently long period is neccessary. This chapter deals with the experimental procedure and results of photometer inter-comparison conducted in Bremen.

3.1 Instrumentation

(a) Isometric view **(b)** Front view **(c)** With PoE and housing

Figure 3.1: SQM-LE night sky luminance photometer.

The instruments used for night sky luminance measurement were two Sky Quality Meters with lens and Ethernet (SQM-LE) manufactured by Unihedron[1], as shown in Figure 3.1. SQM-LE operates by counting incoming photons using a light to frequency converter (TAOS TSL237[2]), a silicon photodiode which converts the photon signal into photocurrent. A current to frequency converter then converts the

[1]For details see `http://www.unihedron.com/projects/sqm-le/`

[2]Specifications can be found in `http://www.taosinc.com/downloaddetail.aspx?did=120`

photocurrent into a frequency signal, which is proportional to the magnitude of the photocurrent. This frequency signal is then used by the SQM-LE's microcontoller to calculate the sky luminance, which is temperature-corrected using the output of the temperature sensor on the circuit of the SQM-LE. The microcontroller of the SQM-LE calculates the luminance in two modes. When the integration frequency is low, it calculates the luminance from the integration time of the photodiode for each cycle, and it measures the integration frequency when the integration time is short. The SQM-LE outputs the readings in luminance in the unit of magnitude per square arcsecond (Mag/Arcsec^2), number of cycles with the period of its internal clock, frequency and integration time. It also outputs the circuit temperature. The manufacturer claims that the uncertainty is 0.10 Mag/Arcsec^2 (approximately 11%). The Ethernet port enables the SQM-LE to be connected to the network so that data acquisition through the network is possible.

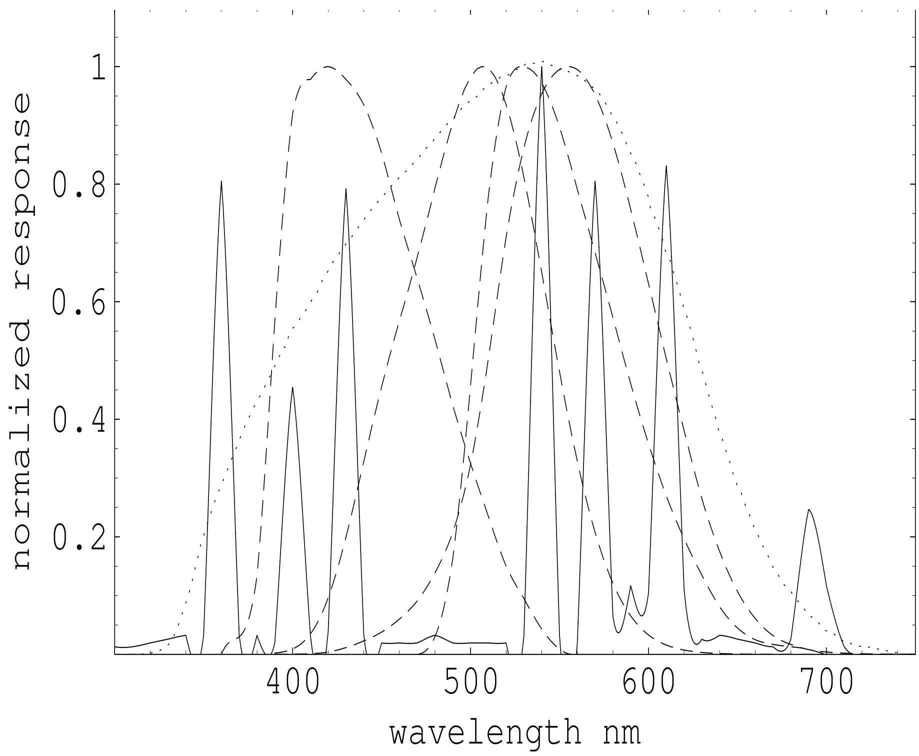

Figure 3.2: Relative spectral response of SQM (dotted), which is essentially the same as the SQM-LE used here but without the lens. Also shown in the graph are (dashed lines, from left to right) Johnson B-band, CIE scotopic band, Johnson V-band and CIE photopic band. The spectrum of a high pressure sodium (HPS) lamp is shown in solid line [2].

The SQM-LE has a focusing lens which narrows the field of view. Its full-width half-maximum (FWHM) field of view, according to the specifications of the manufacturer, is 20°. In front of the silicon photodiode a Hoya CM-500 IR-cutting filter is placed to reduce the unwanted IR signal [2]. The spectral response of the SQM-LE can be found in Figure 3.2. Also shown in the figure are the curves of Johnson B-band and Johnson V-band, which are the standards in wideband measurements of stellar objects in astronomy [10], the CIE scotopic band and CIE photopic band, which are the modeled response of the human eye [4]. The spectrum of a typical high pressure sodium (HPS) lamp, which is a common type of lighting used for street illumination, is also shown.

The SQM-LE itself is not a waterproof device, which necessitates the use of a waterproof housing provided by the manufacturer. It is essentially a PVC tube with caps at the both ends. On the top side a glass window with a diameter of 43 mm is attached with silicone sealant. The attenuation of the glass window is 0.11 Mag/arcsec^2 according to the manufacturer's specification. A feedthrough is provided at the bottom for network and/or power cables. The body of the housing is around 80 mm in diameter, which can also accommodate a power-over-Ethernet (PoE) splitter chosen by the manufacturer. The PoE connection method is used considering the long running length of cable needed at the measurement sites, and due to electrical safety reason. Figure 3.3 shows an SQM-LE in use.

Figure 3.3: SQM-LE in use.

3.2 Measurement Site

The measurement site is situated in the campus of the University of Bremen, on the flat roof of the Naturwissenschaften 1 (NW1) Building. The university itself is situated in the district of Horn-Lehe, which is approximately 5 km from the city center district. The geolocational data for the site, measured using a GPS receiver, is shown in Table 3.1.

Table 3.1: Geolocational data for measurement site NW1, University of Bremen.

Latitude	Longitude	Elevation (m)
53.1038° N	8.8498° E	22

(a) 1st setup

(b) 2nd setup

Figure 3.4: Mounting of SQM-LEs.

The measurement site was chosen such that the field of view for the instruments could be maximized, but no significantly strong direct light sources would reach the instruments and induce additional measurement uncertainty.

3.3 Installation of SQM-LEs and Data Acquisition

In order to perform inter-comparison of the SQM-LEs and night sky luminance measurment simultaneously, both of the SQM-LEs were installed at the measurement site. Initially, the two SQM-LEs were mounted on the fence side-by-side with hose clamps and cable ties. However, this initial mounting method was not stable and could easily be tilted by strong winds (shown in Figure 3.4a. This was because the SQM housings were supported by the fence at only one point. Therefore, a second mounting method, shown in Figure 3.4b, was used. Using this mounting method, the tilting problem of the housing was eliminated. The SQM housings were aligned to the zenith so that no significant visual angular deviation from the zenith was observed.

A dedicated computer was used as a listener to SQM-LEs and as a data server for sky luminance readings. Using a modified Perl script originally provided by the manufacturer, data request was sent to each SQM-LE through the network once every minute, and the datastream was recorded in plain text files, one for each individual photometer. The real-time clock of the computer was synchronized using NTP server through the Internet. Figure 3.5 shows the connection scheme of the SQM-LEs during the inter-comparison.

The period of inter-comparison started from the evening of 7-12-2011 and ended in the morning of 6-2-2012 with the old firmware, and from 9-2-2012 to 23-2-2012 for the new firmware. In total approximately 87,000 measurements from the old firmware and 25,500 measurements from the new firmware were made by each of the instruments, including data taken during the daytime.

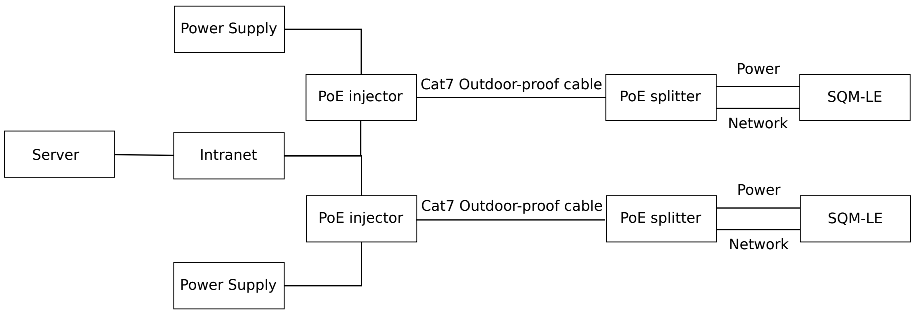

Figure 3.5: Schematic diagram of SQM-LE network setup during inter-comparison.

3.4 Measurement of Attenuation of Housing Glass Window

To verify whether the attenuation coefficient of the glass window on the housing cover complied with the stated value by the manufacturer, a simple setup of a calibration box was made. The design was similar to that used by the BMP project [6], except that the light source was a incandescent light instead of LEDs. A teaching-grade luxmeter with an uncertainty of $\pm 10\,\text{lux}$ was used for checking the stability of the light source. The setup is shown in Figure 3.6.

The whole setup was put into a dark room. Readings were taken every 2 s and 120 readings were taken from each of the SQM-LE with the glass window. Then another 120 readings for each device were taken without the glass window. Finally the positions of the 2 SQM-LEs were swapped and 120 readings were taken again for each device, with the glass windows on, in order to minimize the uncertainty arisen by possible geometric inaccuracy.

The result of the measurement is shown in Table 3.2. It can be seen that the deviation of the attenutation values of the two glass windows are very small compared with the instrumental uncertainty of the SQM-LEs ($0.10\,\text{Mag/Arcsec}^2$). Nevertheless, the

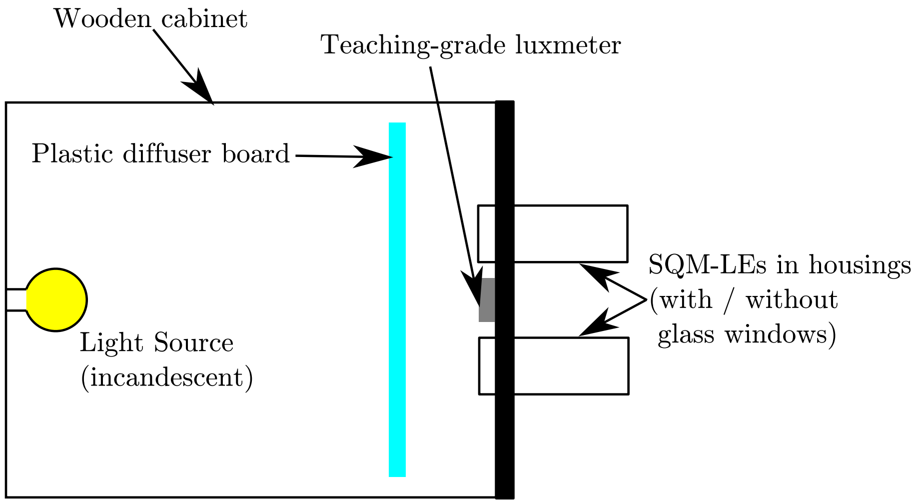

Figure 3.6: Schematic diagram of calibraion box.

obtained attenuation values were applied to the readings in order to minimize the systematic uncertainty from the glass window attenuation.

Table 3.2: Results for Glass Window Attenuation Test.

SQM serial nr.	Mean glass window attenuation [Mag/Arcsec^2]
1760	0.0998±0.0026
1786	0.1167±0.0041

3.5 Data Analysis

Data points were filtered by moon elevation angle and measured luminance value for the scatter plot of the inter-comparison.

During the inter-comparison campaign, it was observed that at high moon elevation angle, the discrepancies in readings between both SQM-LEs were significant, in both setups shown in Figures 3.4a and 3.4b. An example is shown on Figure 3.7. Since a high correlation of the discrepancy occurrence and the lunar elevation was found after checking the time series, all data taken when moon elevation angle was higher than -2°, estimated using Python package PyEphem[3], were filtered out.

Also, since for the NW1 building, luminance values above 15 Mag/arcsec^2 were not observed under normal conditions (i.e. not under thunderstorm, strong point source, etc.), only data points with a luminance of darker than 14 Mag/arcsec^2 were used for data analysis.

[3] http://rhodesmill.org/pyephem/

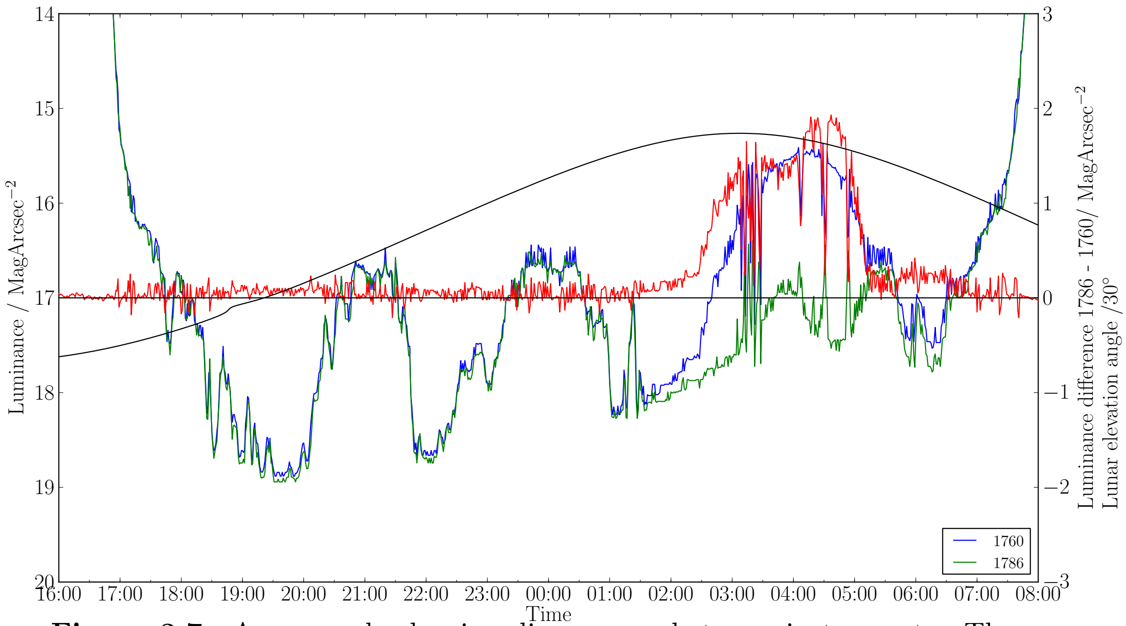

Figure 3.7: An example showing discrepancy between instruments. The black line represents the lunar elevation angle, and the red line is the difference between the instrument readings.

A Python routine using the packages Numpy, Scipy and Matplotlib was used to produce the scatter plots for the luminance readings from both of the devices. A scatter plot was generated for each of the inter-comparison dataset taken with old firmware and new firmware. The unweighted linear least-squared fit, the RMS error and the correlation coefficient were calculated.

3.6 Results and Discussion

The results of the inter-comparison using both the old and new firmware are shown in Figure 3.8.

Since MPSAS Magnitude is a logarithmic unit, the slope of the fit is the linearity factor, which means that the relationship between the two SQM-LEs' readings are exactly linear, when the slope is exactly at unity. And the y-intercept is the scaling factor, which means that the scaling between the two devices is unity when the y-intercept is exactly zero.

From the results using both the old and new firmware, it can be noted that the linearity between the two devices are very high as the slope is close to unity. Also, their scaling agree well with each other.

It can be noticed from Figure 3.8a that clouds of data points are present in the scatter plot when using the old firmware, and the cloud size is proportional to the

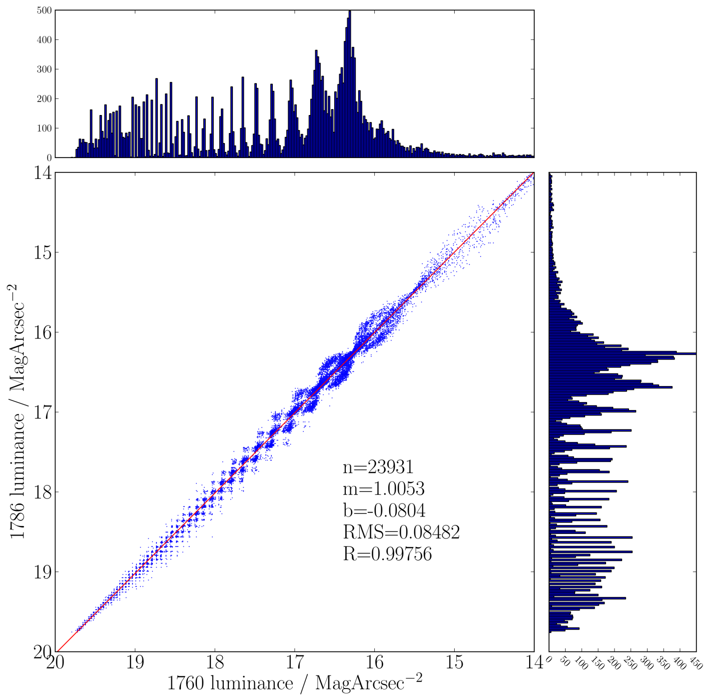

(a)

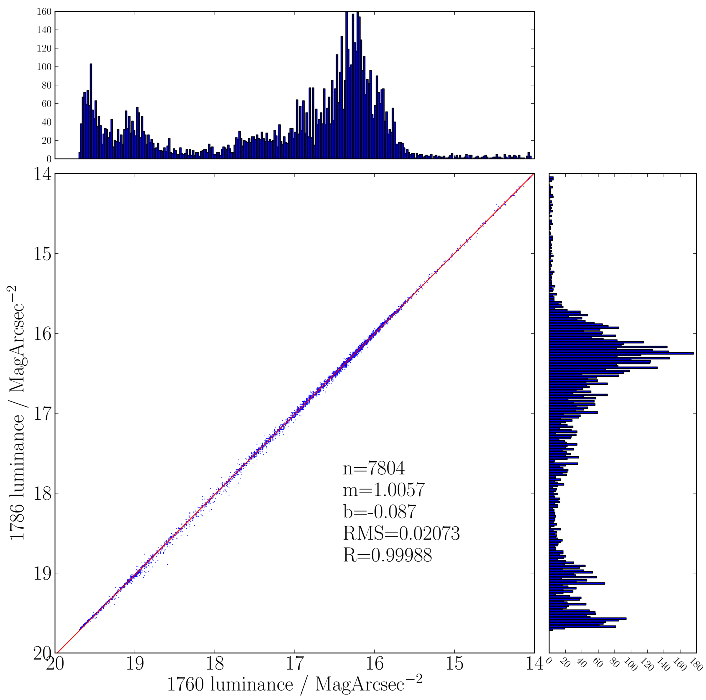

(b)

Figure 3.8: Scatter plots for Bremen SQM-LEs using (a) old firmware and (b) new firmware.

luminance value. This was caused by the quantization artifact of the SQM-LEs when using the old firmware, leading to the much higher RMS error. Details will be discussed in the Section 4.2.3.

Since the performance of both SQM-LEs were similar, assigning inter-calibration factors for the SQM-LEs are not necessary, and the readings of the two devices are compared directly.

Chapter 4

Analysis of Dataset outside Bremen

In analyzing night sky luminance data from other cities, one can have an overview of the situation of light pollution around the world. This is useful in a way that local data can be classified and compared for evaluation of the environmental impact. This chapter describes the data analysis procedure for an international measurement campaign of night sky luminance using SQMs.

4.1 Measurement Campaign of International SQM Survey

The International SQM Survey was an effort conducted by C.C.M. Kyba of the Institute for Space Sciences, Freie Universität Berlin for measuring the zenith night sky luminance at sites around the world. The measurement sites are situated in areas of various types land uses, including urban, suburban and rural areas, and some sites were pristine, which are situated in areas where no significant anthropogenic light source are present within 50 km. Each of the sites was equiped with an SQM with computer or network connectivity, and the zenith night sky luminance was measured continuously.

Table 4.1: List of International SQM Survey sites.

Site ID	Site name	Country	Latitude (°)	Longitude (°)	Elevation (m)	Site type
3	Arkemheen	The Netherlands	52.2500	5.4300	4	rural
6	Berlin_Dahlem	Germany	52.4577	13.3107	91	urban
7	Berlin_Babelsberg	Germany	52.4046	13.1016	66	suburban
8	bmp1	Italy	43.4100	10.4200	15	unknown
9	bmp2	Italy	45.7080	11.6794	87	unknown
10	bmp3	Italy	45.0802	11.5598	9	unknown
11	bmp4	Italy	45.4688	11.3505	212	unknown
12	bmp5	Italy	46.0112	12.3130	500	unknown
13	CESAR	The Netherlands	51.9700	4.9300	2	rural
15	DeerLick2	USA	33.5576	-82.7626	192	pristine
16	Hamilton	Canada	43.2687	-79.9596	99	suburban
17	Springendal	The Netherlands	52.4300	6.8800	74	rural
19	RadioKootwijk	The Netherlands	52.1100	5.4900	71	rural
20	Schiermonnikoog	The Netherlands	53.4800	6.200	7	rural
21	Schipluiden	The Netherlands	51.9900	4.2800	1	rural
22	trueblood	USA	31.6656	-110.6018	1516	rural
23	unihedron	Canada	43.1844	-79.5206	173	suburban
24	Utrecht	The Netherlands	52.0800	5.1100	6	urban
26	Vlaardingen	The Netherlands	51.9100	4.3200	4	suburban

In total, there were 26 sites participating the campaign. The data owners of 19 of the sites granted permission of using the data for this study, all of which from the Northern Hemisphere. The detailed list of dataset owners used in this study can be found in Appendix B, and a summary of locations of the measurement sites is shown in Table 4.1 and Figure 4.1.

Depending on measurement sites, the housing used by each individual device and the measurement interval vary. The attenuation values of the housing windows were recorded in at least 8 known cases by the data owners, who determined the values experimentally. For sites without measurement of housing window attenuations, an attenuation value was assumed to be 0.11 Mag/Arcsec^2 if the housing assembled by the SQM manufacturer was used. The interval between two consecutive measurements ranged between 1 s and approximately 15 minutes. To avoid systematic uncertainty arisen by possible seasonal dependence of atmospheric and astronomical parameters, as well as those from human activities, all measurements were made within the same period. The chosen period for the datasets was between May and September, 2011, when the difference in the equation of time (difference the apparent solar time and the true time) between the extrema was around 15 minutes, lower than the annual difference of 30 minutes.

4.1.1 Investigation of Amplification Effect by Reflection of Clouds - Cloud coverage analysis

It is a well known effect that clouds reflects anthropogenic lights, which give the typical reddish color during cloudy nights in areas with high anthropogenic light emissions. Kyba et al. [12] quantified this cloud amplification effect in Berlin using two SQMs. In their study, it was found that the cloud amplification is proportional to the intensity of anthropogenic light.

In order to verify if this applies to other locations around the world, similar procedures were applied to the International SQM Survey dataset. For the data of the whole period, only the data within 15 minutes from the calculated local true midnight were used, as suggested by Kyba et al. in [12]. Also, as discussed in the previous chapter, moonlight could cause the SQMs output data with large discrepancy when the lunar elevation angle was high. Therefore, data points were not used when the lunar elevation angle exceeded 2° below the horizon. In addition, only data points with SYNOP[1] cloud observations within 30 minutes were selected. This resulted in a smaller, but potentially more consistent dataset.

[1]FM-12 SYNOP (Synoptic surface observation) is an alphanumeric code standardized by the World Meteorological Organization (WMO) for reporting surface weather from a manned or automatic fixed land station. Detailed information of the code can be found on [35].

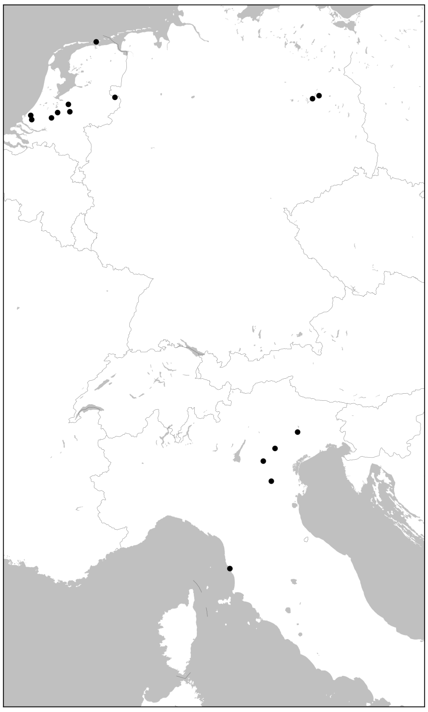

(a) Europe

(b) North America

Figure 4.1: Map of International SQM Survey sites. Locations are marked with black dots.

4.1.2 Change of Sky Luminance during the Night - Average night sky luminance time series

Also from their study of Berlin's night sky, Kyba et al. [12] found that as the night progressed, the zenith night sky luminance decreased in average. The exact cause of this trend is still unknown, but is believed to be related to human activities or the change of thickness of the atmospheric boundary layer (ABL) [19].

Since the length of period required for observing the change of sky luminance during the course of night was longer than that for finding the amplification effect of clouds as discussed on Section 4.1.1, the time filtering criterion used by observing amplification of cloud was replaced by a solar elevation filtering criterion. Instead of filtering the data by time of measurement, only data points were kept when the solar elevation was below 16° below the horizon. The criterion for lunar elevation screening remained the same value of -2°.

4.2 Data Analysis

4.2.1 Preprocessing for Raw Datasets

Since the raw datasets for all the sites were in different formats (all of which ASCII), including the choice of delimiter, time stamps and headers, in order to simplify the process for data analysis, these raw datasets were first unified to a common file format, which consisted of unix time, UTC time, raw luminance reading in Mag/Arcsec^2 and device temperature, all fields separated by space characters.

After unification of dataset formats, minute-by-minute mean luminance values were taken, time stamp being aligned to the 30th second of the minute. The time of real local midnight was calculated for each site by finding the annual mean time of solar anti-transit (the time when the solar elevation angle reached the minimum), neglecting the equation of time, and the hours after local real midnight was calculated for each minute-by-minute mean measurement. Solar elevation angles, lunar elevation angles were calculated using PyEphem as well. The number of measurement within the averaged minute, the instrumental uncertainty and the statistical uncertainty were also recorded. The data after the preprocessing was written into a common ASCII, space-separated file, using a location ID number to distinguish between the sites.

4.2.2 Data Reduction and Processing for Cloud Coverage Analysis and Night Time Cloud-free Time Series

The SYNOP data were obtained through the website OGIMET[2]. For each of the dataset, the SYNOP site was chosen based on the proximity from the measurement site and the frequency of cloud observations. The observation interval ranged from 1 hour to 6 hours. The cloud coverage in oktas was assumed to be constant within 30 minutes from the time of observation, and therefore the cloud coverage was not interpolated between two observations.

As discussed in the Section 4.1, two different reduced data subsets were used for cloud coverage analysis and average cloud-free time series. For the cloud coverage analysis, measurement time filter and lunar elevation angle filtering were carried out. Each dataset was first classified according to the reported cloud coverage in oktas, then for each subset of different cloud coverage, the median and the overall uncertainty were calculated. In the average cloud-free time series, solar elevation angle and lunar elevation angle filtering were performed, and only data points which were reported to be cloud-free were used. Then for each 5-minute interval, the median value and overall uncertainty over all observed cloud-free nights were found when the sample size within that interval was at least 2.

4.2.3 Error Analysis

There are three main sources of uncertainties in the analyzed data, namely the manufacturer's claimed device uncertainty for all models of SQMs (0.10 Mag/Arcsec^2), the uncertainty arisen from reading quantization using the old version of firmware specific to the model SQM-LE, and statistical uncertainty of measurements. Here the latter two sources of uncertainties will be discussed.

Quantization Artifacts in SQM-LEs

It is found by many users that using the SQM-LE's firmware of older versions, a noticeable quantization artifact can be observed, an example of which is shown in Figure 3.8a. The artifact is present when the SQM-LE calculates the luminance in integration time mode, and is more significant when luminance is high. This artifact disappears when the SQM-LE switches from integration mode to frequency mode for luminance measurement. The switching point may vary from device to device. For the devices used in this study, all except three devices were found to exhibit quantization artifacts when raw luminance reading were darker than 15 Mag/Arcsec^2, and the rest did not show any artifact. This might be caused by higher sensitivities of the

[2] `http://www.ogimet.com`

photodiode used in the three devices of concern, which would lead to a much darker switching point[3]. The exact origin of this artifact is still unknown, but is believed to be caused by the combination of electromagnetic interference (EMI) and the inverse proportionality between the uncertainty of measurement and the integration time [4].

Using the Bremen dataset acquired during the inter-comparison campaign before the application of the new firmware, the positions of the peaks were first determined by visual check of the histogram with the raw luminance reading ranging between 18.5 Mag/Arcsec^2 and 15.5 Mag/Arcsec^2. Then the first guess of peak-to-peak distance with respect to the raw luminance reading was modeled by an exponential function. The peak detection window was then set to half the distance between peaks. This peak detection function was then applied to the International SQM datasets, except those which did not show significant quantization artifacts. After the peaks were found for all datasets used, the mean of the distances of the considered peak to its left and right neighbors were first determined, and by visual check, peaks which were not detected correctly were excluded. Finally with all the peak distance data between 20 Mag/Arcsec^2 and 15 Mag/Arcsec^2 from all datasets used (the lower limit of 20 Mag/Arcsec^2 was used because quantization artifact was not visible on all dataset at low light readings), an unweighted quadratic fit was done. The quantization uncertainty with respect to raw luminance reading is then half the fitted peak distance, and for the raw luminance readings darker than the minimum of the quadratic fit (in this case at about 19.5 Mag/Arcsec^2), the quantization uncertainty is assumed to be the same as that at the turning point, i.e. close to 0.01 Mag/Arcsec^2. The results are shown in Figure 4.2 and Table 4.2. Since the average RMS error of 0.014 Mag/Arcsec^2 is far below the manufacturer's claimed uncertainty of 0.10 Mag/Arcsec^2, This fit will be used on all device except the three which did not show quantization artifacts for the rest of the analysis in this study.

Table 4.2: RMS error by luminance reading for quantization uncertainty fit.

Raw luminance reading (Mag/Arcsec^2)	RMS error
19.5 - 20.0	0.0039
19.0 - 19.5	0.0044
18.5 - 19.0	0.006
18.0 - 18.5	0.0092
17.5 - 18.0	0.0131
17.0 - 17.5	0.0203
16.5 - 17.0	0.0299
16.0 - 16.5	0.0566
15.5 - 16.0	0.0813
15.0 - 15.5	0.1083

To address the problem arisen by quantization artifacts, a new firmware was developed by the manufacturer. The new firmware takes the average of the last 8

[3]Personal communication with Anthony Tekatch, Unihedron, 3-8-2012

[4]Personal communication with C.C.M. Kyba, Freie Universität Berlin

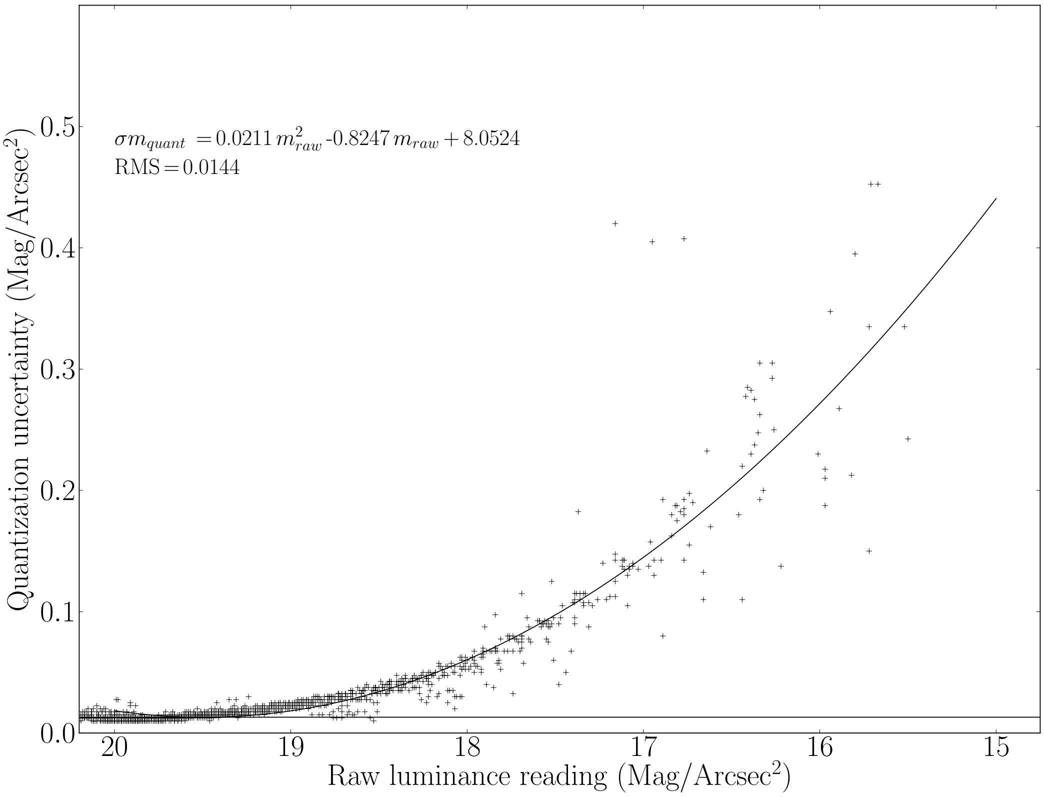

Figure 4.2: The resulting fit for the quantization uncertainty. The horizontal black line represents the minimum of the quadratic equation, which is used as the quantization uncertainty darker than the turning point.

readings when running in integration time mode[5]. This effectively eliminates the quantization artifact, as can be seen in Figure 3.8b. Therefore, for the data taken with the new firmware, the quantization uncertainty is assumed to be zero.

Statistical Uncertainty of Measurements

Since the cloud data come from SYNOP stations, in some cases more than 60 km away from the measurement sites, a difference between the cloud coverage at the SYNOP station and that of the measurement site may arise. Also, the optical thickness of clouds, which determines the reflectance of anthropogenic lights emitted from the ground, depends greatly on the composition of the droplets and the size of the droplets [31], which in turn depends on the atmospheric condition around the measurement sites. Therefore even under an overcast sky, it can be expected that variations in reflectance of clouds are present. Furthermore, since the difference in optical thickness between clouds and clear skies is large, it can also be expected that when the sky is scattered with clouds, the variation in the sky luminance increases as well.

[5]Personal communication with Anthony Tekatch, Unihedron, 11-5-2012.

Combining Uncertainties for Analyses

Assuming that the measurement in glass window attenuation has a negligible uncertainty, then for the i-th instantaneous night sky luminance observation, m_i, the associated instrumental uncertainty, $\sigma_{m,i}$, can be written as

$$\sigma_{m,i} = \sqrt{\sigma_{m,ma}{}^2 + \sigma_{m,i,qu}{}^2} \tag{4.1}$$

where $\sigma_{m,ma}$ and $\sigma_{m,i,qu}$ are the manufacturer's claimed uncertainty and the quantization uncertainty associated to the measurement dependent on the raw luminance reading, respectively. It should be noted that the quantization uncertainty is assumed not to vary from device to device, as a single quadratic equation was used to fit the peak distance with respect to raw luminance readings in Section 4.2.3. Also, when the reading is made by the new firmware, $\sigma_{m,i,qu}$ should be assigned zero.

With this uncertainty assigned to all single instantaneous obsrervations, the uncertainty of any minute-by-minute mean, m_{1min}, with M measurements, can be expressed as

$$\sigma_{m,1min} = \sqrt{\frac{1}{M}\sum_{i=1}^{M} \sigma_{m,i}{}^2 + \sigma_{m,1min,geo}{}^2} \tag{4.2}$$

where $\sigma_{m,1min,geo}$ is the geophysical uncertainty for the mean luminance in the averaged minute, arisen by variation of sky luminance due to e.g. change of cloud coverage, cloud reflectance or other parameters for atmospheric conditions, as discussed in section 4.2.3. Expanding this equation using Equation 4.1 yields

$$\begin{aligned} \sigma_{m,1min} &= \sqrt{\frac{1}{M}\sum_{i=1}^{M} \left(\sigma_{m,ma}{}^2 + \sigma_{m,i,qu}{}^2\right) + \sigma_{m,1min,geo}{}^2} \\ &= \sqrt{\sigma_{m,ma}{}^2 + \frac{1}{M}\sum_{i=1}^{M} \sigma_{m,i,qu}{}^2 + \sigma_{m,1min,geo}{}^2} \end{aligned} \tag{4.3}$$

From this equation we can see that the manufacturer's claimed uncertainty remains after taking minute-by-minute average.

Also, in practice, for about half the number of the sites, the measurement intervals were longer than 1 minute. In these cases, the geophysical variation is no longer known. Mathematically this means $\sigma_{m,1min,geo} = 0$, and Equation 4.2 becomes

$$\sigma_{m,1min} = \sqrt{\frac{1}{M}\sum_{i=1}^{M} \sigma_{m,i}{}^2}.$$

Finally, for an averaged luminance of any data subset, $\overline{m}$, with N 1-minute average values, the total uncertainty can be estimated by

$$\sigma_{\overline{m}} = \sqrt{\frac{1}{N}\sum_{j=1}^{N} \sigma_{m,1min,j}{}^2 + \sigma_{\overline{m},geo}{}^2}. \tag{4.4}$$

Again $\sigma_{\overline{m},geo}$ is the geophysical uncertainty among the N minute-by-minute measured average luminance. Adding this term is necessary because the RMS of $\sigma_{m,1min,geo}$ does not necessarily reflect all the contribution of the geophysical variation. This can be demostrated by an extreme example where variation among the minute-by-minute average luminances exists, but no variation within each of the minute-by-minute observations. In this case, the RMS of $\sigma_{m,1min,geo}$ is zero, but $\sigma_{\overline{m},geo}$ is not. Inserting Equation 4.3 into this equation, all the contributing terms of uncertainties can be clearly seen:

$$\begin{aligned}
\sigma_{\overline{m}} &= \sqrt{\frac{1}{N}\sum_{j=1}^{N}\left(\sigma_{m,ma}{}^2 + \frac{1}{M_j}\sum_{i=1}^{M_j}\sigma_{m,i,qu,j}{}^2 + \sigma_{m,1min,geo,j}{}^2\right) + \sigma_{\overline{m},geo}{}^2} \\
&= \sqrt{\sigma_{m,ma}{}^2 + \frac{1}{N}\sum_{j=1}^{N}\left(\frac{1}{M_j}\sum_{i=1}^{M_j}\sigma_{m,i,qu,j}{}^2 + \sigma_{m,1min,geo,j}{}^2\right) + \sigma_{\overline{m},geo}{}^2} \\
&= \sqrt{\underbrace{\underbrace{\sigma_{m,ma}{}^2}_{\text{Manufacturer}} + \underbrace{\frac{1}{N}\sum_{j=1}^{N}\frac{1}{M_j}\sum_{i=1}^{M_j}\sigma_{m,i,qu,j}{}^2}_{\text{Quantization}}}_{\text{Instrumental}} + \underbrace{\frac{1}{N}\sum_{j=1}^{N}\sigma_{m,1min,geo,j}{}^2}_{\text{1-minute geophysical}} + \underbrace{\sigma_{\overline{m},geo}{}^2}_{\text{Subset geophysical}}}
\end{aligned} \tag{4.5}$$

Obviously when the other uncertainties are absent, the total uncertainty reduces to the manufacturer's claimed uncertainty, $\sigma_{m,ma}$, of 0.10 Mag/Arcsec^2.

4.3 Results and Discussion

4.3.1 Cloud coverage analysis

Table 4.3: Summary of Results for cloud coverage analysis of International SQM Survey for selected sites where clear sky and overcast sky data are both available. For detailed description of the sites see Table 4.1. All luminances and uncertainties are in Mag/Arcsec^2.

		Clear sky			Overcast sky		
Site ID	Site type	Data count	Luminance	Uncertainty	Data count	Luminance	Uncertainty
3	rural	694	20.295	0.350	792	19.069	0.664
6	urban	425	19.168	0.184	125	16.577	0.333
7	suburban	360	20.123	0.159	336	17.794	0.421
9	unknown	128	19.560	0.526	6	17.515	0.295
13	rural	636	20.279	0.321	720	19.100	0.566
15	pristine	958	21.280	0.300	120	21.530	0.388
17	rural	446	20.973	0.283	695	20.680	0.504
19	rural	120	20.721	0.118	283	20.397	0.707
20	rural	149	20.678	0.246	120	21.474	0.531
21	rural	494	18.614	0.494	661	16.067	1.113
24	urban	20	18.970	0.122	30	16.290	0.964
26	suburban	495	17.356	0.264	603	16.040	0.708

A summary of cloud coverage analysis is shown in Figure 4.3 and Table 4.3. For more detailed cloud coverage analysis of each single site see Appendix A.

12 out of the 19 sites used in this study collected both clear and overcast sky data. Most of these sites are situated in the rural areas, and 4 sites are in urban or suburban areas. In general, with the notable exception of site 21 (Schipluiden, The Netherlands), most of the sites situated in rural areas were darker than those inside or near the cities.

Under clear sky, the urban or suburban sites could be brighter than 19.1 Mag/Arcsec^2. In contrast, most of the sites in rural areas were darker than 20 Mag/Arcsec^2. Under cloudy sky, most of the sites except sites 15 (DeerLick2, DeerLick Astronomy Village, USA) and 20 (Schiermoonikoog, The Netherlands), had brighter skies than that under a clear skies. This can be expected because when the intensity of anthropogenic light is much stronger than the natural sky, the reflections of light from the clouds become significant. When the sites are far away from any anthropogenic light source like site 15, then the blockage of natural night sky light sources by the clouds is more significant than reflections of anthropogenic light source from the ground. Therefore these sites show a darker sky during the cloudy nights.

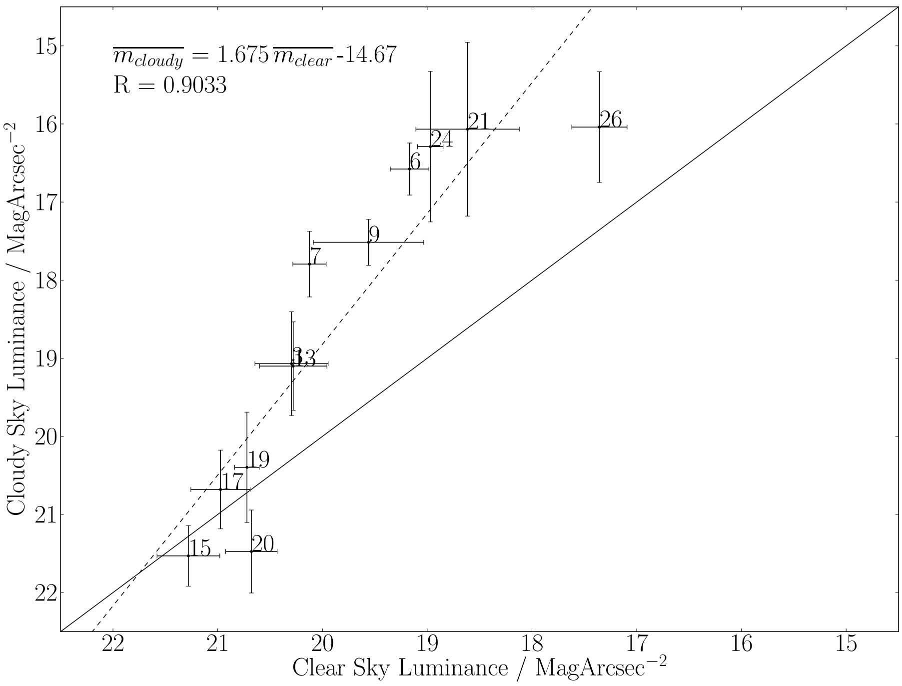

Figure 4.3: Overcast sky luminance against clear sky luminance scatter plot as shown in Table 4.3, labelled with site ID. Dashed line is the linear fit of the available dataset. A 1:1 line (solid), meaning no cloud amplifcation, is also plotted.

Figure 4.3 shows a clear increasing trend in cloudy night sky luminance with respect to clear night sky luminance. Although not lying at the linear fit, the points of cloudy sky luminance with respect to clear sky luminance lie around the linear fit with a slope of 1.68 and with a correlation of around 90%. This means that the amplification of anthropogenic light by clouds increases with the intensity of emitted light from the ground level, as already demonstrated in the study of Kyba et al. in Berlin [12]. It should be noted that the data of site 26 (Vlaardingen, The Netherlands) lies far away from the linear fit. Although it was much brighter than the other sites under clear sky observed in this study, the cloudy sky was only approximately as bright as other urban or suburban sites. This particular site lies in a very busy area of ports and factories, and a large city, Rotterdam, also lies not far away. It is suspected that direct light from street lamps around the site, as well as the floodlights used by sports fields, might enter the device, negating the cloud amplification. This remains to be investigated.

Although site 20 is situated in rural area, it was brighter than most of the urban and suburban sites. This might be explained by the fact that this site is located in an area of greenhouses[6]. Since in the Netherlands, most greenhouses keep their lightings on during the night, they may contribute a great portion of anthropogenic light. Even if the light shades are appropriately designed in a way that most of the

[6]Personal communication with Dorien Lolkema, RIVM

lights are directed downwards, the reflection from the plants may still be significant. This may change the night sky luminance tremendously.

From Appendix A, the median luminance against cloud coverage plots show fluctuations for cloud coverage between 1 and 7 oktas, especially for those datasets from rural areas. This might be the result of insufficient sample size (in most cases less than 90 minute-by-minute observations, corresponding to 3 nights if measurement interval is 1 per minute or more) and variation of cloud reflectance, combined with the relatively weak anthropogenic light source from the ground level. Also from the results of median luminance against cloud coverage, it can be seen that for most of the time, the geophysical variation among minute-by-minute observations are the most dominant factor of all the sources of uncertainty, except when the statistics are small. Considering that the sky luminance can vary by up to factor of tens, the instrumental uncertainty and the geophysical variations within individual minutes can be safely neglected when statistics is large.

4.3.2 Average night sky luminance time series

The average clear night sky luminance time series for individual sites are presented together in Appendix A. Over more than half of the sites, a decreasing trend in zenith night sky luminance during the course of the night could be observed. However, since for some of the SYNOP stations used for filtering out luminance data taken during cloudy condition only make observations less than every hour, and in the worst case once every six hours, they may not represent the true temporal variation in night sky luminance of the sites.

It may be noted also for site 21, a very pronounced increasing trend in night sky luminance is observed as the night progresses. Whether this is related to the pattern of usage of plant lights in the greenhouses, as discussed in the previous subsection, remains to be investigated.

Chapter 5

Night Sky Monitoring in Bremen

This chapter describes the experimental procedures and analysis of results for the night sky monitoring campaign in Bremen and its neighboring rural area.

5.1 Methodology

The two SQM-LEs involved in the inter-comparison campaign described in Chapter 3 were used in the night sky monitoring campaign. One of the devices (Serial nr. 1786) remained at the same position on the roof of the NW1 Building in the campus (site name Bremen_Horn-Lehe), while the other device (Serial nr. 1760) was moved to the rural site located in Seebergen near Lilienthal, Lower Saxony (site name Bremen_Seebergen). The data of the measurement sites is shown in Table 5.1.

Table 5.1: List of Bremen night sky monitoring sites.

Site	Latitude (°)	Longitude (°)	Elevation (m)	Site type
Bremen_Horn-Lehe	53.1038	8.8498	22	suburban
Bremen_Seebergen	53.1363	8.9851	11	rural

The device on the roof of NW1 was mounted as shown previously in Figure 3.4b, and the device in Seebergen was set up outside of a family house and mounted on a wooden pole as shown in Figure 5.1. The data was transferred through the Internet to the data server.

The data processing and analysis procedure was similar to that used in Chapter 4, except that the measurement started from 8-12-2011 at the campus site, and from 27-2-2012 at the rural site. Also, from 9-2-2012, readings were made by the new firmware of SQM-LE, and the quantization uncertainty is neglected for those readouts, as discussed in Section 4.2.3. Luminance reading was requested from each

(a) (b)

Figure 5.1: Setup of SQM-LEs at the rural site in Seebergen, Lilienthal.

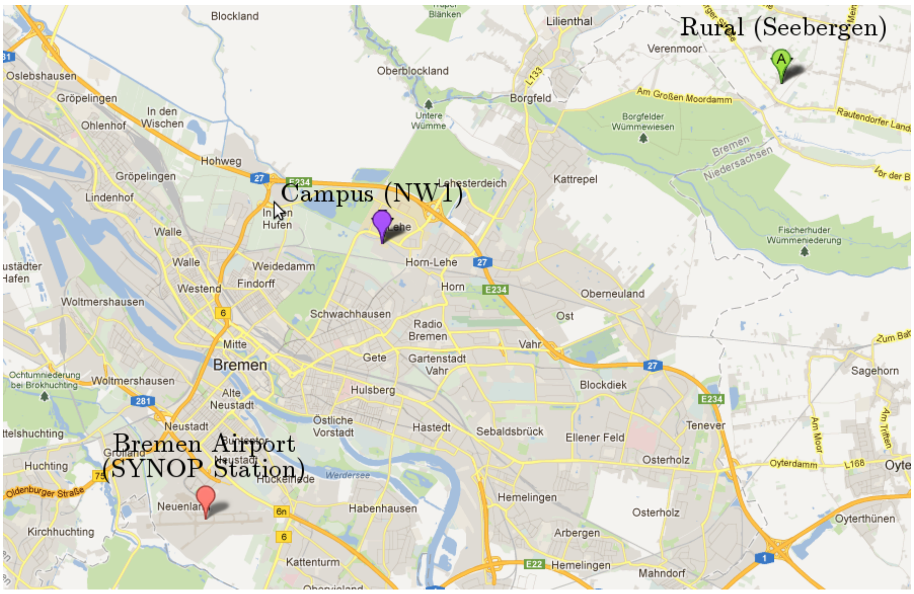

Figure 5.2: A map showing the measurement sites in Bremen and the used SYNOP station (using Google Maps).

device by a Python script once every minute. The data from the SYNOP station of Bremen City Airport (WMO index 10224), situated in the district of Neuenland at the southern part of Bremen, was used for cloud coverage data. It is situated southwest of the measurement sites, 7.4 km from the campus site and 16.1 km from the rural site. A map showing the positions of the sites and the SYNOP station can be found in Figure 5.2.

5.2 Results and Discussion

5.2.1 Cloud coverage analysis

Tables 5.2 and Figure 5.3 show the results of cloud coverage analysis for the Bremen datasets. Table 5.3 lists the unitless linear cloud amplification factor with respect to cloud coverage in oktas. In total, 3349 and 1068 minute-by-minute observations were made for the campus and rural sites, respectively. Considering that the measurement period is 30 minutes per night, this would mean a total of 111.6 and 35.6 observed nights in the campus and respectively the rural sites.

Table 5.2: Results for cloud coverage analysis of Bremen dataset. All luminance values and uncertainties are given in unit of Mag/Arcsec^2. Note that no minute-by-minute geophysical uncertainty is present since data was taken once per minute.

(a) Campus

Oktas	Data count	Median luminance	Uncertainty: Instrumental	Uncertainty: Subset geophysical	Uncertainty: Total
0	362	19.355	0.100	0.228	0.249
1	210	19.390	0.100	0.616	0.624
2	300	19.350	0.101	0.358	0.372
3	300	19.590	0.100	0.717	0.724
4	60	19.210	0.102	0.394	0.407
5	90	19.175	0.100	0.520	0.529
6	186	18.705	0.100	0.763	0.769
7	1279	17.140	0.129	0.834	0.843
8	562	16.530	0.138	0.559	0.576

(b) Rural

Oktas	Data count	Median luminance	Uncertainty: Instrumental	Uncertainty: Subset geophysical	Uncertainty: Total
0	176	20.845	0.100	0.090	0.135
1	84	20.960	0.100	0.158	0.187
2	90	20.725	0.100	0.190	0.215
3	148	20.755	0.100	0.430	0.442
4	30	20.710	0.100	0.135	0.168
5	30	20.465	0.100	0.074	0.125
6	60	20.600	0.100	0.175	0.201
7	330	19.855	0.100	0.477	0.488
8	120	20.410	0.100	0.203	0.226

Table 5.3: Linear cloud amplification factors for Bremen dataset.

(a) Campus

Oktas	Amplification factor
1	0.968 ± 0.538
2	1.005 ± 0.662
3	0.805 ± 0.494
4	1.143 ± 0.644
5	1.180 ± 0.584
6	1.820 ± 0.475
7	7.691 ± 0.445
8	13.490 ± 0.561

(b) Rural

Oktas	Amplification factor
1	0.899 ± 0.809
2	1.117 ± 0.792
3	1.086 ± 0.653
4	1.132 ± 0.820
5	1.419 ± 0.844
6	1.253 ± 0.800
7	2.489 ± 0.628
8	1.493 ± 0.785

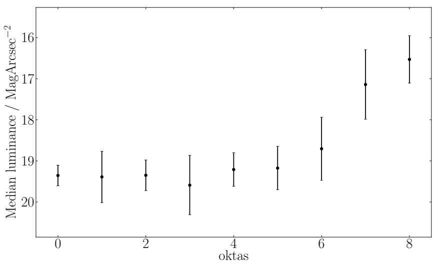

(a) Campus

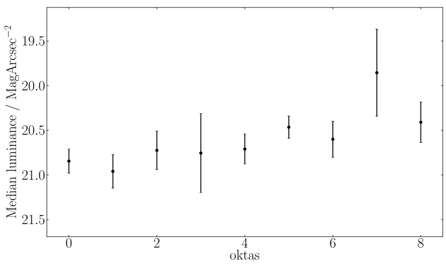

(b) Rural

Figure 5.3: Cloud coverage analysis plot for Bremen dataset as shown in Table 5.2.

From the results it can be clear seen that for the campus site, which is situated in thee suburban area of Bremen, the zenith night sky luminance was higher than that for the rural site in Seebergen, both during clear and cloudy nights. In clear nights, the suburban area of Bremen is approximately 1.5 Mag/Arcsec^2, or a factor of 3.9, brighter than the rural area. During overcast nights an even higher difference of 3.9 Mag/Arcsec^2 (a factor of 36) can be observed.

An enormous difference in linear cloud amplification factor between the campus and rural sites can be found from Table 5.3. The cloud amplification factor of over 13 in the suburban area of Bremen, in contrast less than 1.5 in the rural area, clearly shows the relationship between the intensity of anthropogenic light and the effect of ground level light reflection by the clouds. This finding is consistent with the observations in Chapter 4.

Again, the effect of small statistics on the fluctuation of median luminance for cloud coverage between 1 and 7 can be demostrated in Figure 5.3b. Since there are only 35.6 nights of observations, compared with 111.6 nights at the campus site, the consistency in the increase of zenith sky luminance with respect to cloud coverage is affected. This is easiest to be seen with the luminance data for 7 oktas. In order to get more consistent data, measurement should be continued.

5.2.2 Average night sky luminance time series

The average night sky luminance time series for both the campus and rural sites can be found in Figure 5.4.

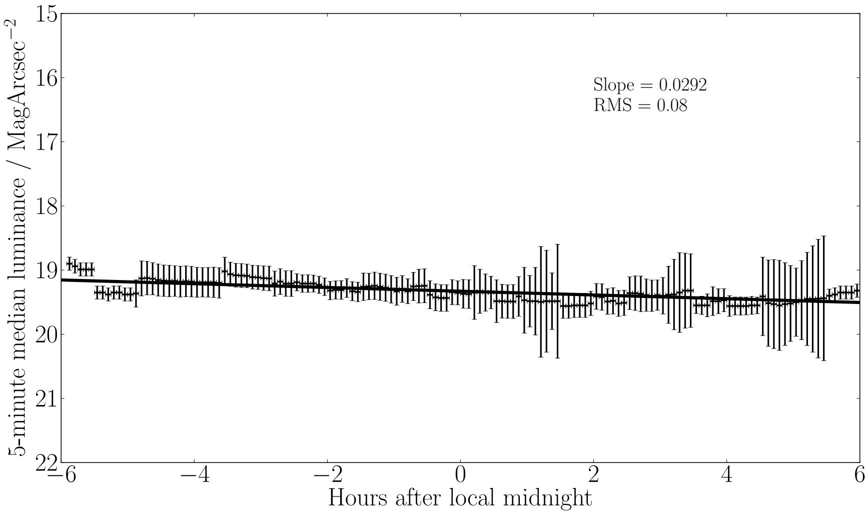

(a) Campus

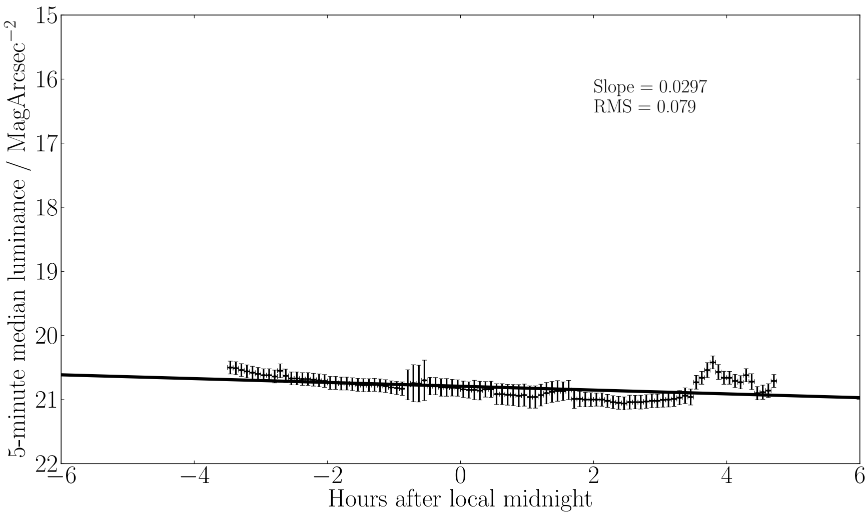

(b) Rural

Figure 5.4: Average night sky luminance time series for Bremen. The quoted slope has a unit of Mag/Arcsec^2.

Both sites show a general trend of weak decrease in zenith sky luminance during the progress of the night. Also seen from the plots is that near the end of the night, both sites show a trend of increase in luminance. It is possible that this might be attributed to the increase of human activities. Also noticable is a sudden postive jump in luminance around 4 hours after local midnight for the rural site. This might be associated with the switching of the street illuminations.

5.2.3 Comparison with International SQM Servey data

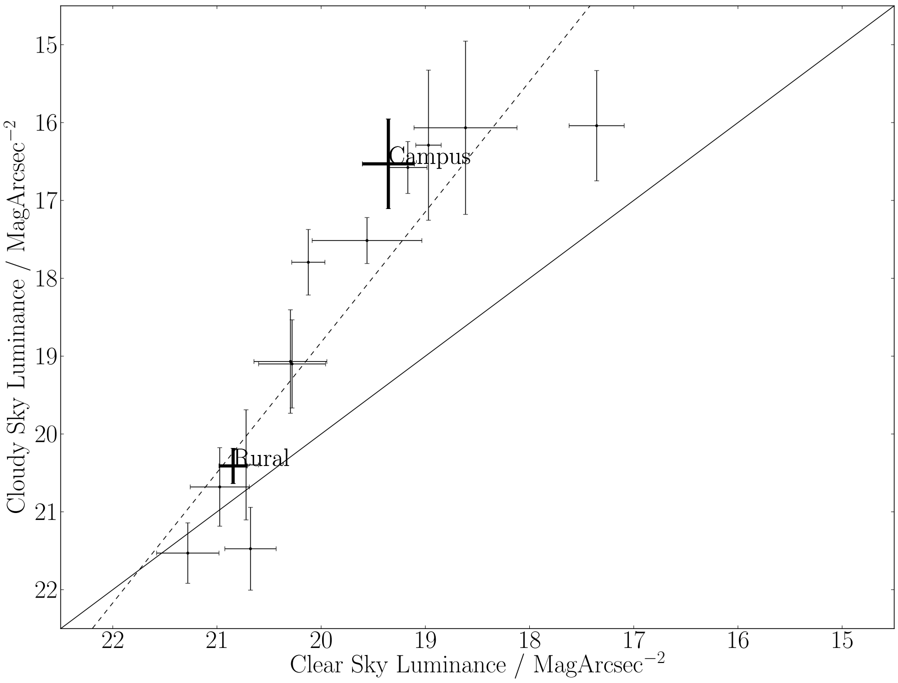

Figure 5.5: Clear sky and overcast sky luminances data of Bremen (bold crosses) superimposed on scatter plot of International SQM Survey dataset as shown in Figure 4.3.

When the luminance data for clear and overcast skies in Bremen is superimposed on the scatter plot for International SQM Survey data, as shown on Figure 5.5, we can confirm that the results of observations in Bremen, both from the campus and rural sites, are consistent with the observations from the other sites around the world. Both observations lie close to the linear fit for the international dataset in the scatter plot. For the campus site dataset, the measured results are typical for urban and suburban area e.g. Berlin, and for the rural site dataset, the results lie within the regime of observed values from other rural sites. With this, we can also confirm that the cloud amplification effects observed from Bremen's suburban and rural areas are similar to those found in other places of the world. However, since the campus site (in the Horn-Lehe District) is not the most densely populated site of the city, it can be expected that if the measurement is made within the city center, an even brighter cloud-free sky and larger cloud amplification can be observed.

With this information, we may expect that the adverse effect on human arisen from light pollution in Bremen will be similar to that in other cities around the world. If the ecological situation of Bremen is known in details, the impact of anthropogenic light on the nature in Bremen as well as its surroundings can be assessed.

Chapter 6

Conclusions

Since there are many adverse effects of light pollution both on human and on the nature it is necessary to conduct studies and measurements in light pollution. Bremen is one of the largest city in Germany, therefore it is expected that the associated problem with light pollution in other large cities can affect Bremen and its surroundings as well. However, there were only limited studies, especially in-situ studies, on this in the past, which means that a more detailed study about the situation of light pollution in Bremen is needed.

Two low-cost photometers, Sky Quality Meters with Lens and Ethernet (SQM-LEs) were used to measure the zenith night sky luminance in the suburban and rural areas of Bremen. Before they were deployed for in-situ measurements, the SQM-LEs were set up at the same place for a two-month inter-comparison of performance. The attenuation of the housing windows used by the devices were also measured with a calibration box. The devices were found to be consistent with each other when measuring in laboratory. However, for observing the sky, differences occurred in the case that the moon was present. This necessiated filtering out data taken when the moon was above.

The data from an international effort for quantifying night sky luminance in different areas around the world, the International SQM Survey, was analyzed in order to understand the general situation of light pollution around the world, and compare the situation of Bremen to those in other regions. It was found that in general, under clear sky the urban and suburban areas are brighter than the rural areas. When clouds are present, the skies are brighter in light-polluted regions, and the difference in zenith night sky luminance between light-polluted areas and non-light-polluted areas becomes larger than that under cloud-free skies. This shows that cloud coverage can affect the extent of light-pollution. Also found from the data analysis was that skies in light-polluted areas are usually darker as night progresses. This may imply that human activities and / or other atmospheric parameters may also be related to the sky luminance.

The findings from the dataset of Bremen's suburban and rural areas are similar to those of the international dataset. The night sky luminance in the suburban area of Bremen is similar to other urban or suburban areas in the world, whereas the situation in Bremen's rural area is also typical for areas with similar land use outside Bremen. With this information at hand, we can expect that the environmental impacts by light pollution in Bremen is also similar to that in the other cities. However, since no ecological information was acquired in this study, the ecological impact cannot be assessed at this stage.

Outlook

Aerosols of different sizes are known to influence the propagation of light in the atmosphere. Works on correlating daytime aerosol optical thickness (AOT) measured by sunphotometer to night sky luminance was initiated, but the statistics is insufficient for the time being. More AOT data will be collected in the future to try to find out their relationships. Also, as the effect of aerosols is dependent on the zenith angle [5], measurements should be done also at oblique angles.

In addition, since the propagation of anthropogenic lights in the atmosphere depends on the spectrum of the light source, and the spectrum of skyglow may change the ecological impact of light pollution [13], there is a need to conduct spectroscopy of the night sky.

With in-situ measurement data on hand, satellite images (e.g. from DMSP/OLS) can be used to correlate the luminance of Bremen's night sky in the present time. After an absolute calibration between the SQM-LEs and the satellite image data, the night sky luminance in the past may also be estimated.

Appendix A

Results for selected International SQM Survey Sites

The following pages show the analyzed data for the cloud coverage analysis and Average night sky luminance time series. All median luminance and uncertainties quoted in the cloud coverage analysis are in the unit of Mag/Arcsec^2. All cloud amplification factors are unitless linear values. The slope quoted in the average cloud-free night sky luminance time series is in the unit of Mag/Arcsec^2 hour.

Arkemheen (Site ID: 3)

Cloud Coverage Analysis

Oktas	Data count	Median luminance	Uncertainty			
			Instrumental	1-minute geophysical	Subset geophysical	Total
0	694	20.295	0.101	0.012	0.335	0.350
1	60	19.259	0.102	0.045	0.705	0.713
4	30	20.442	0.101	0.061	0.294	0.317
6	139	20.262	0.102	0.013	0.689	0.697
7	60	19.711	0.101	0.033	0.507	0.518
8	792	19.069	0.103	0.044	0.655	0.664

Cloud Amplification Factor

Oktas	Amplification factor
1	2.597 ± 0.481
4	0.873 ± 0.647
6	1.031 ± 0.488
7	1.713 ± 0.562
8	3.093 ± 0.501

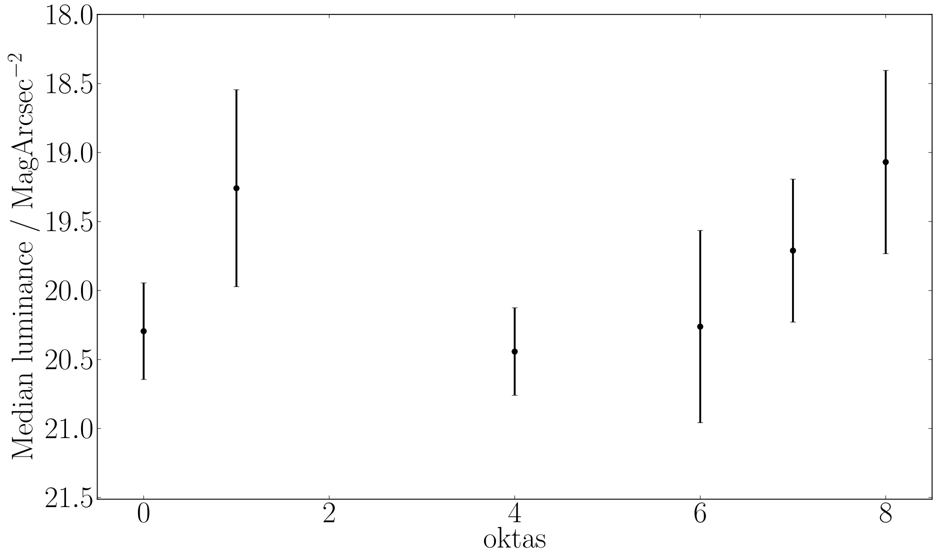

Cloud coverage analysis plot

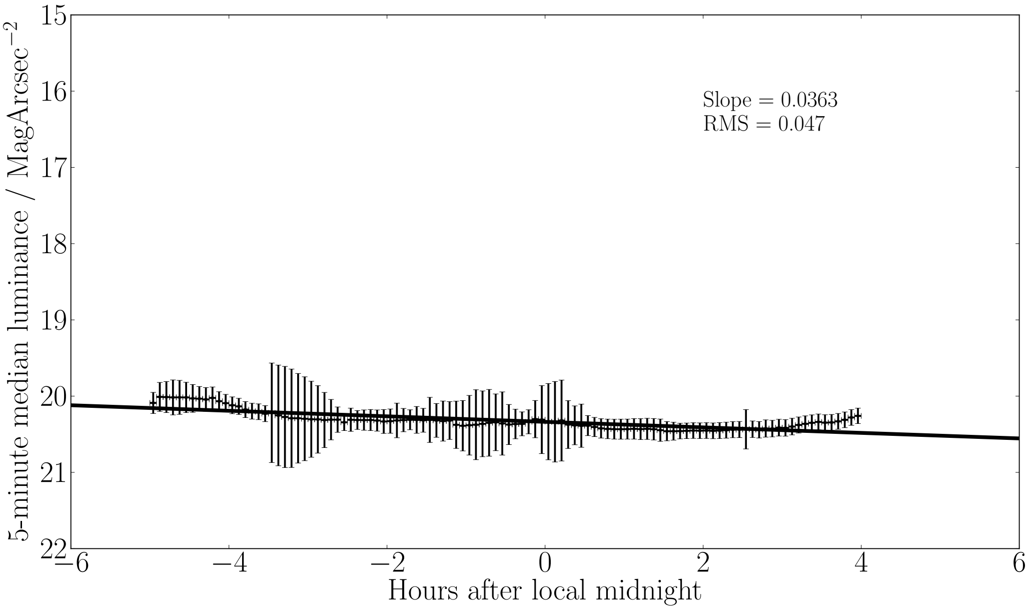

Average cloud-free night sky luminance time series

Berlin_Dahlem (Site ID: 6)

Cloud Coverage Analysis

Oktas	Data count	Median luminance	Uncertainty			
			Instrumental	1-minute geophysical	Subset geophysical	Total
0	425	19.168	0.101	0.011	0.153	0.184
1	360	19.162	0.101	0.013	0.144	0.176
2	120	18.976	0.102	0.028	0.357	0.372
3	60	18.839	0.113	0.053	0.612	0.625
4	58	18.413	0.118	0.087	0.645	0.662
5	90	17.546	0.155	0.071	0.743	0.763
6	93	18.282	0.113	0.062	0.419	0.438
7	353	16.833	0.181	0.091	0.604	0.637
8	125	16.577	0.209	0.081	0.247	0.333

Cloud Amplification Factor

Oktas	Amplification factor
1	1.006 ± 0.791
2	1.193 ± 0.682
3	1.354 ± 0.549
4	2.004 ± 0.531
5	4.454 ± 0.486
6	2.261 ± 0.645
7	8.593 ± 0.543
8	10.873 ± 0.704

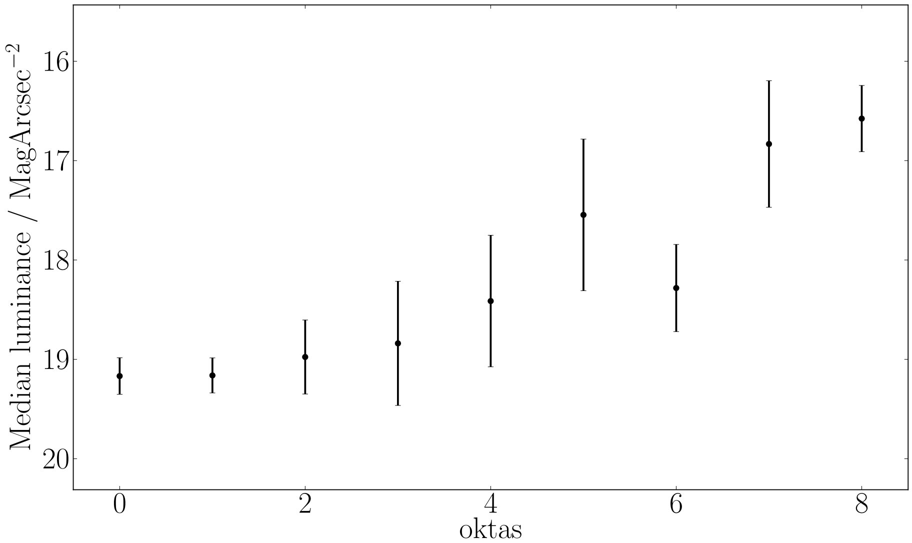

Cloud coverage analysis plot

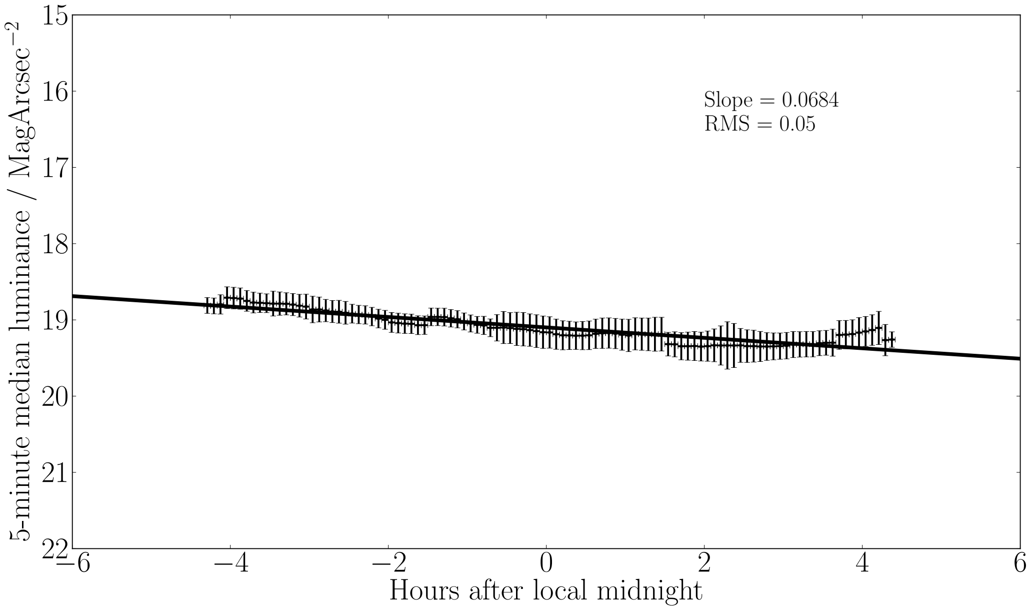

Average cloud-free night sky luminance time series

Berlin_Babelsberg (Site ID: 7)

Cloud Coverage Analysis

Oktas	Data count	Median luminance	Uncertainty			
			Instrumental	1-minute geophysical	Subset geophysical	Total
0	360	20.123	0.101	0.014	0.122	0.159
1	370	20.095	0.101	0.016	0.429	0.441
2	173	20.139	0.101	0.015	0.163	0.192
3	150	19.995	0.101	0.020	0.283	0.302
4	150	19.457	0.101	0.019	0.478	0.489
5	132	18.961	0.102	0.042	0.573	0.583
6	150	19.040	0.104	0.057	0.556	0.569
7	321	18.529	0.109	0.059	0.638	0.650
8	336	17.794	0.120	0.057	0.399	0.421

Cloud Amplification Factor

Oktas	Amplification factor
1	1.026 ± 0.649
2	0.985 ± 0.795
3	1.125 ± 0.730
4	1.848 ± 0.623
5	2.917 ± 0.573
6	2.713 ± 0.580
7	4.344 ± 0.540
8	8.545 ± 0.661

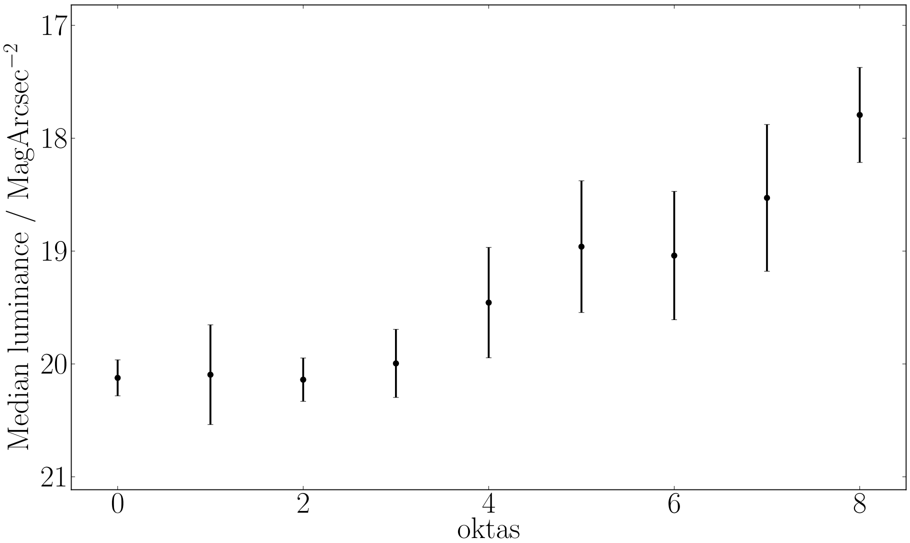

Cloud coverage analysis plot

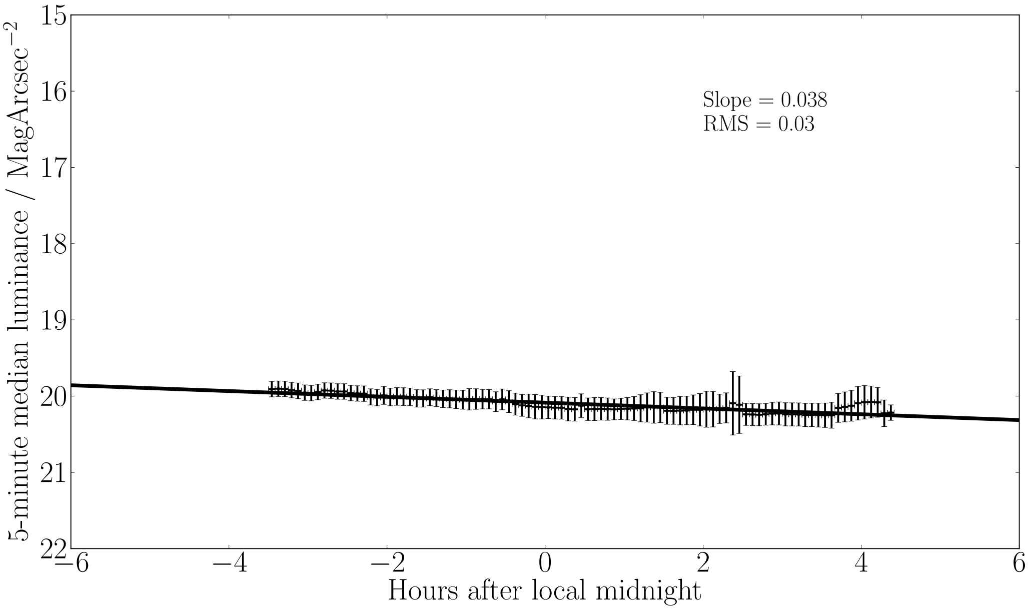

Average cloud-free night sky luminance time series

bmp1 (Site ID: 8)

Cloud coverage analysis and cloud amplification factor: No data

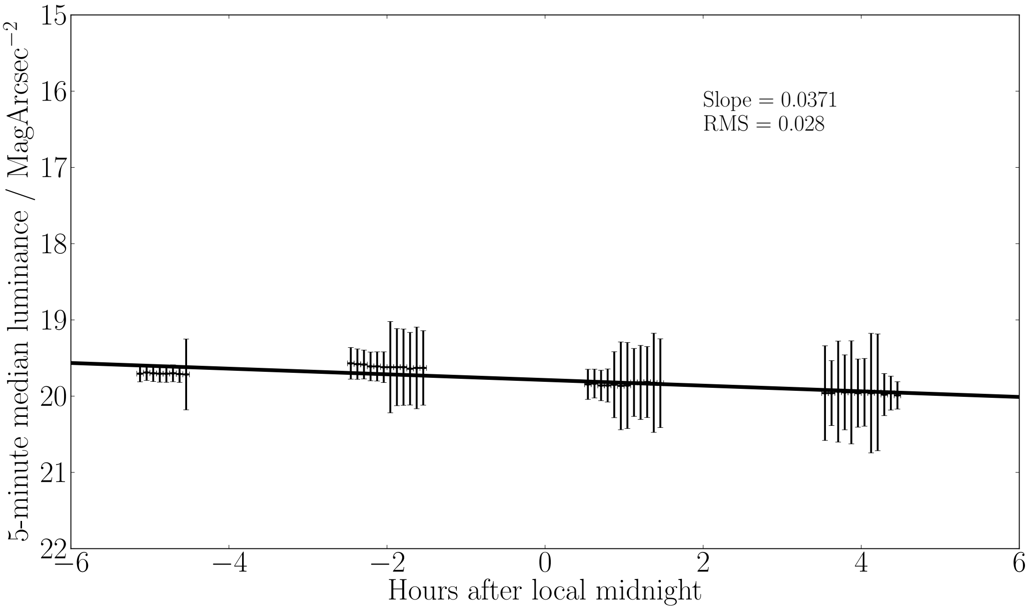

Average cloud-free night sky luminance time series

bmp2 (Site ID: 9)

Cloud Coverage Analysis

Oktas	Data count	Median luminance	Uncertainty			
			Instrumental	1-minute geophysical	Subset geophysical	Total
0	128	19.560	0.103	0.000	0.516	0.526
1	6	19.460	0.101	0.000	0.424	0.436
2	18	18.570	0.111	0.000	0.879	0.886
3	12	18.670	0.118	0.000	0.954	0.962
4	29	18.090	0.116	0.000	0.903	0.911
5	50	18.510	0.109	0.000	0.718	0.727
6	42	17.430	0.138	0.000	0.304	0.334
7	24	17.750	0.129	0.000	0.780	0.791
8	6	17.515	0.132	0.000	0.264	0.295

Cloud Amplification Factor

Oktas	Amplification factor
1	1.096 ± 0.533
2	2.489 ± 0.387
3	2.270 ± 0.364
4	3.873 ± 0.380
5	2.630 ± 0.438
6	7.112 ± 0.563
7	5.297 ± 0.417
8	6.577 ± 0.574

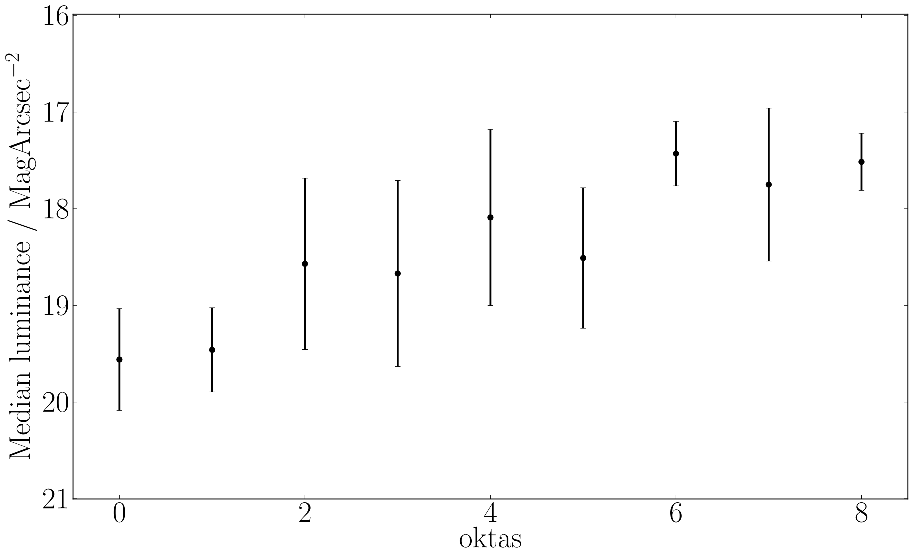

Cloud coverage analysis plot

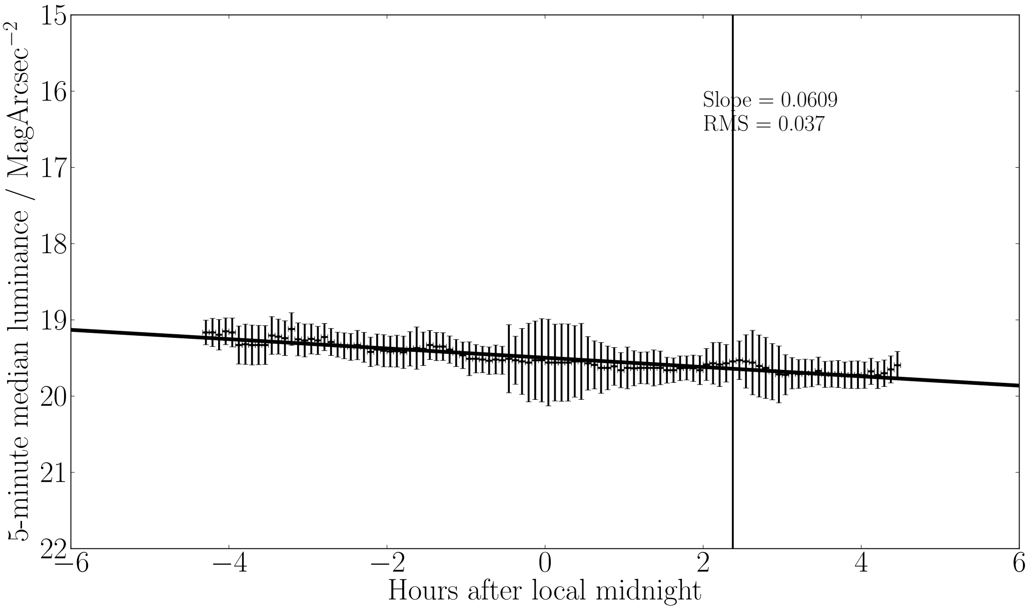

Average cloud-free night sky luminance time series[1]

[1]The long vertical line at 2.375 hours after midnight was caused by abnormal variation of luminance, possibly due to measurement error.

bmp3 (Site ID: 10)

Cloud coverage analysis and cloud amplification factor: No data

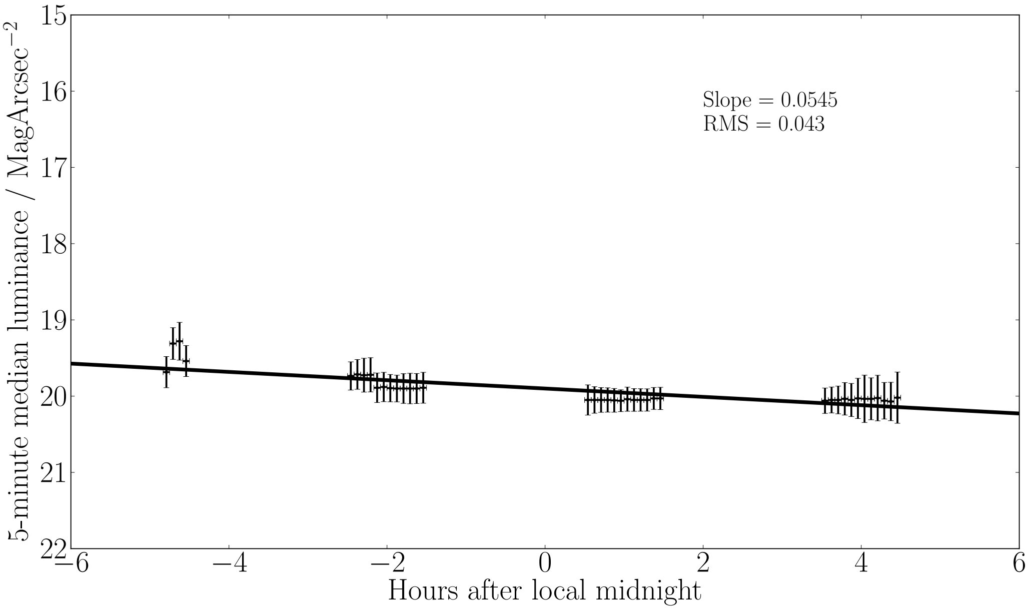

Average cloud-free night sky luminance time series

bmp4 (Site ID: 11)

Cloud coverage analysis and cloud amplification factor: No data

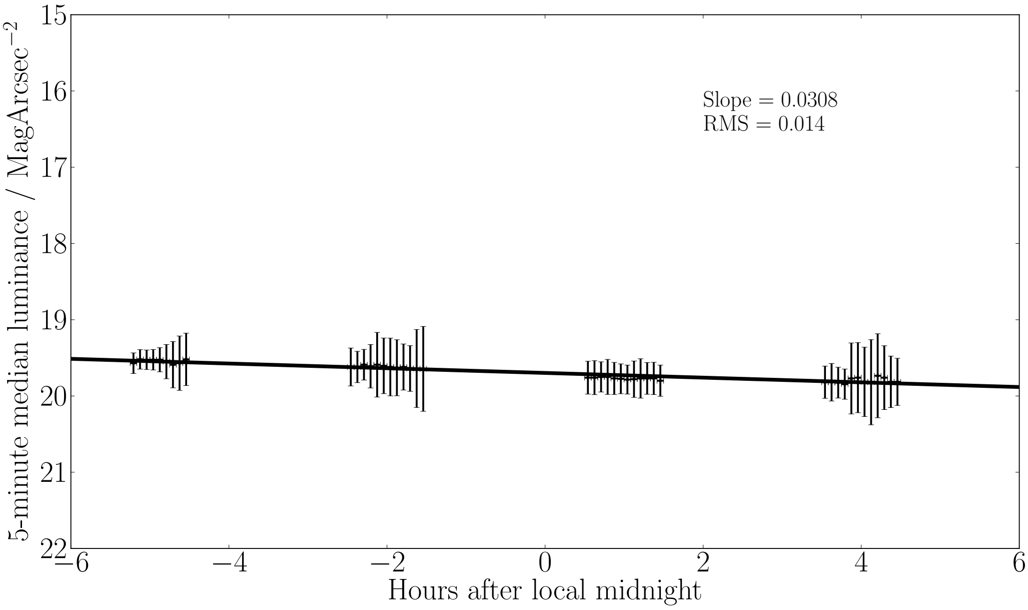

Average cloud-free night sky luminance time series

bmp5 (Site ID: 12)

Cloud coverage analysis and cloud amplification factor: No data

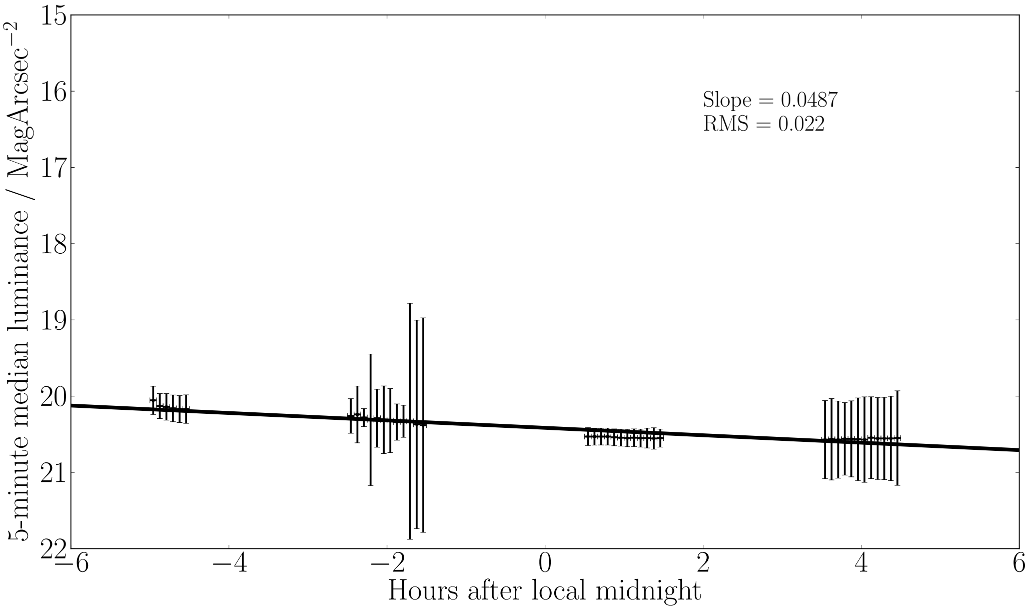

Average cloud-free night sky luminance time series

CESAR (Site ID: 13)

Cloud Coverage Analysis

Oktas	Data count	Median luminance	Uncertainty			
			Instrumental	1-minute geophysical	Subset geophysical	Total
0	636	20.279	0.101	0.013	0.305	0.321
1	243	20.258	0.101	0.013	0.554	0.563
2	45	20.232	0.101	0.037	0.227	0.251
3	60	20.090	0.101	0.016	0.401	0.414
4	58	20.002	0.101	0.020	0.390	0.403
5	30	19.657	0.101	0.034	0.244	0.266
6	120	19.454	0.101	0.074	0.467	0.483
7	120	19.753	0.101	0.034	0.519	0.530
8	720	19.100	0.104	0.108	0.546	0.566

Cloud Amplification Factor

Oktas	Amplification factor
1	1.019 ± 0.550
2	1.045 ± 0.687
3	1.190 ± 0.617
4	1.291 ± 0.622
5	1.774 ± 0.681
6	2.138 ± 0.586
7	1.623 ± 0.565
8	2.963 ± 0.549

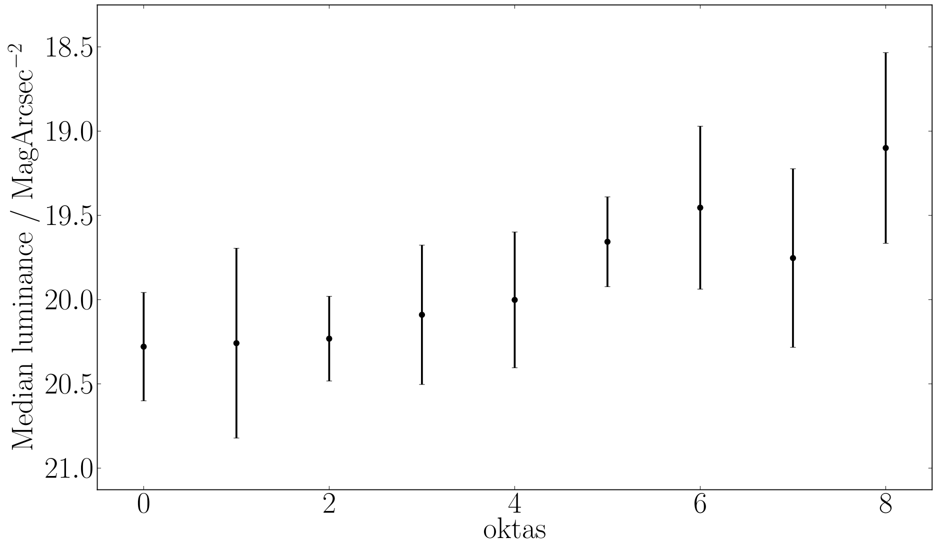

Cloud coverage analysis plot

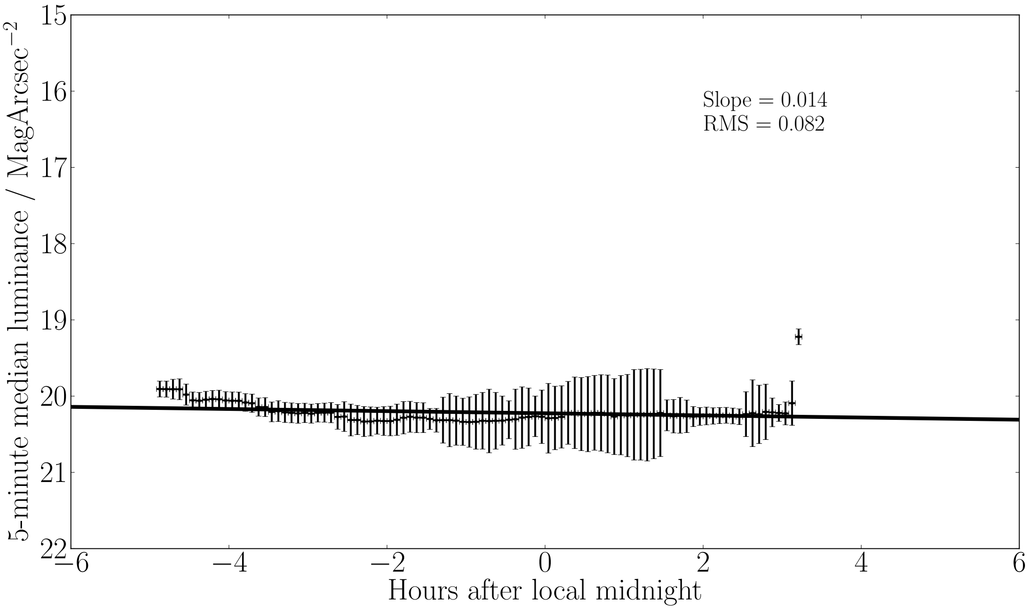

Average cloud-free night sky luminance time series

DeerLick2 (Site ID: 15)

Cloud Coverage Analysis

Oktas	Data count	Median luminance	Uncertainty			
			Instrumental	1-minute geophysical	Subset geophysical	Total
0	958	21.280	0.101	0.000	0.282	0.300
2	90	21.250	0.101	0.000	0.132	0.166
4	60	21.180	0.101	0.000	0.102	0.144
6	30	21.255	0.101	0.000	0.049	0.112
8	120	21.530	0.101	0.000	0.375	0.388

Cloud Amplification Factor

Oktas	Amplification factor
2	1.028 ± 0.729
4	1.096 ± 0.736
6	1.023 ± 0.745
8	0.794 ± 0.637

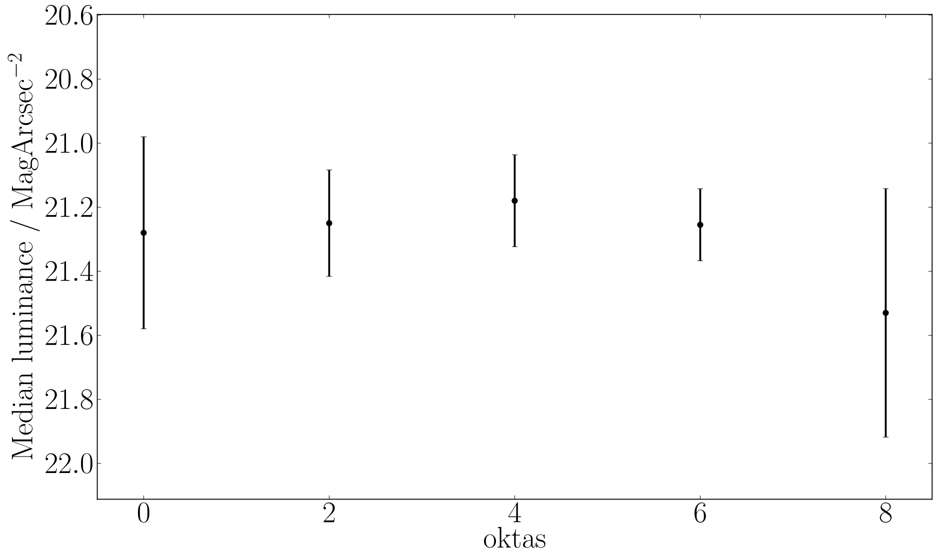

Cloud coverage analysis plot

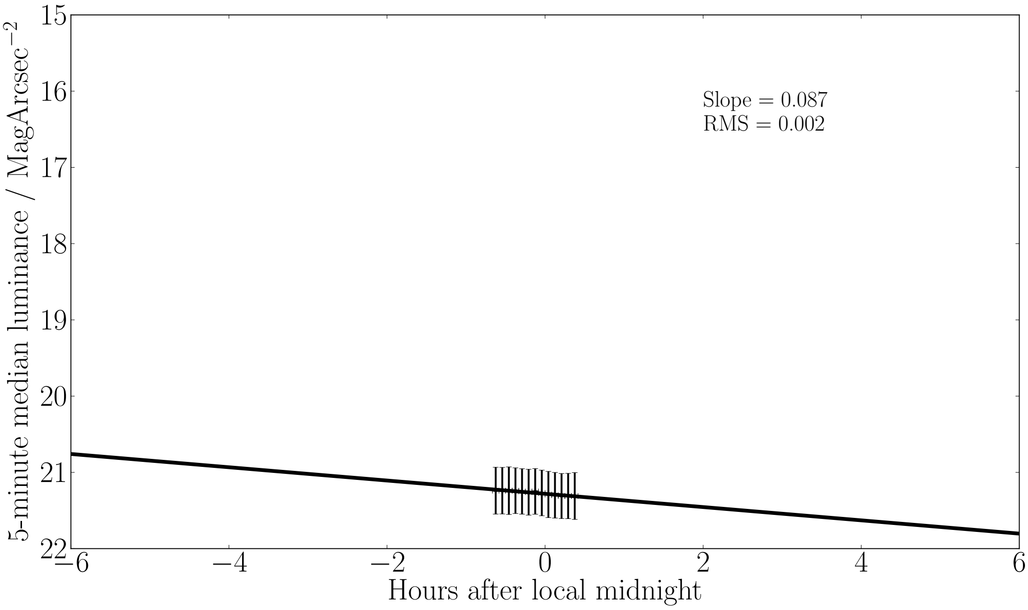

Average cloud-free night sky luminance time series

Hamilton (Site ID: 16)

Cloud coverage analysis and cloud amplification factor: No data

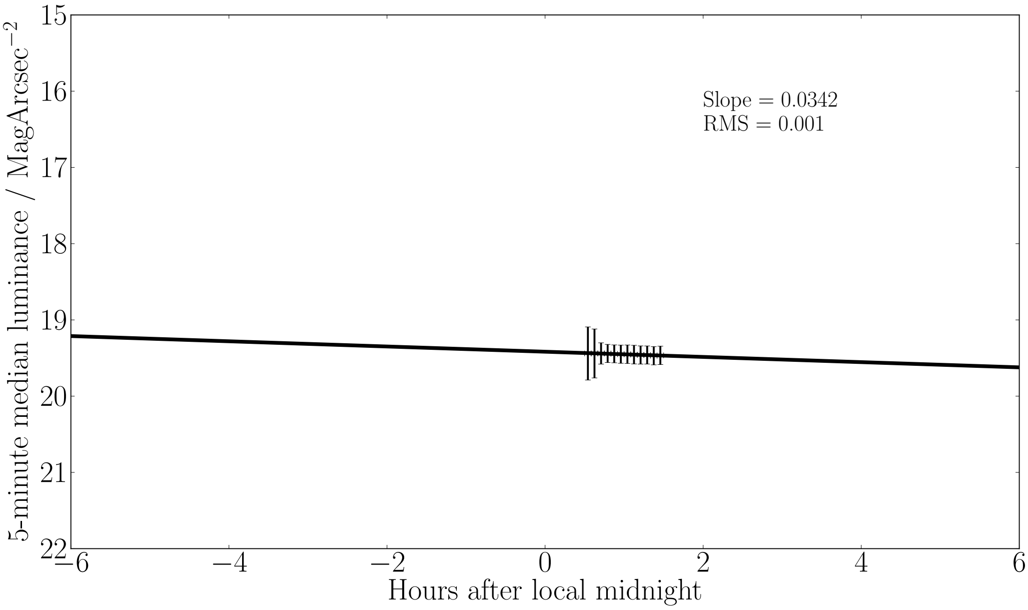

Average cloud-free night sky luminance time series

Springendal (Site ID: 17)

Cloud Coverage Analysis

Oktas	Data count	Median luminance	Uncertainty			
			Instrumental	1-minute geophysical	Subset geophysical	Total
0	446	20.973	0.101	0.007	0.265	0.283
1	120	21.158	0.101	0.015	0.224	0.246
2	30	20.641	0.101	0.010	0.058	0.117
3	60	20.648	0.101	0.011	0.056	0.116
4	90	21.160	0.101	0.011	0.192	0.217
5	80	21.057	0.101	0.017	0.305	0.321
6	60	20.906	0.101	0.013	0.123	0.160
7	210	20.724	0.101	0.031	0.423	0.436
8	695	20.680	0.101	0.030	0.493	0.504

Cloud Amplification Factor

Oktas	Amplification factor
1	0.843 ± 0.708
2	1.358 ± 0.754
3	1.349 ± 0.754
4	0.842 ± 0.720
5	0.926 ± 0.674
6	1.064 ± 0.741
7	1.258 ± 0.619
8	1.310 ± 0.587

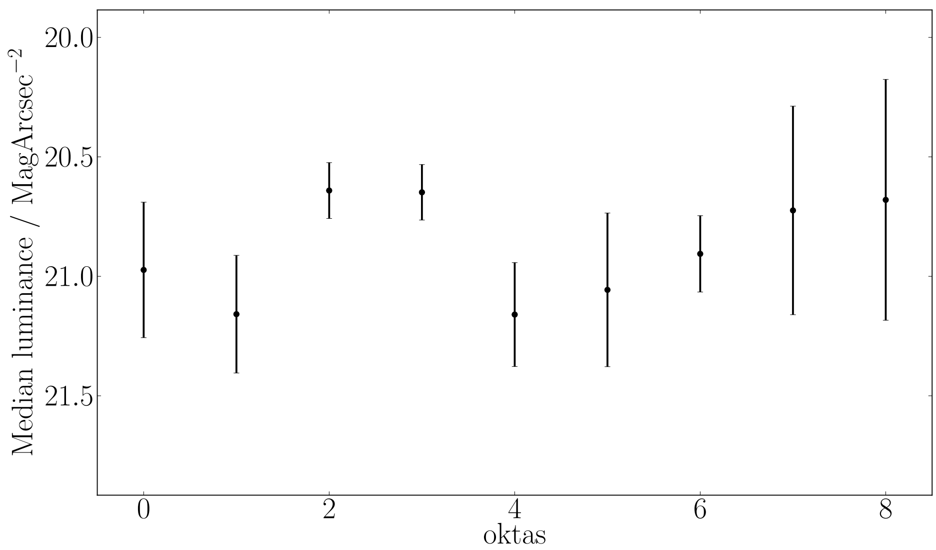

Cloud coverage analysis plot

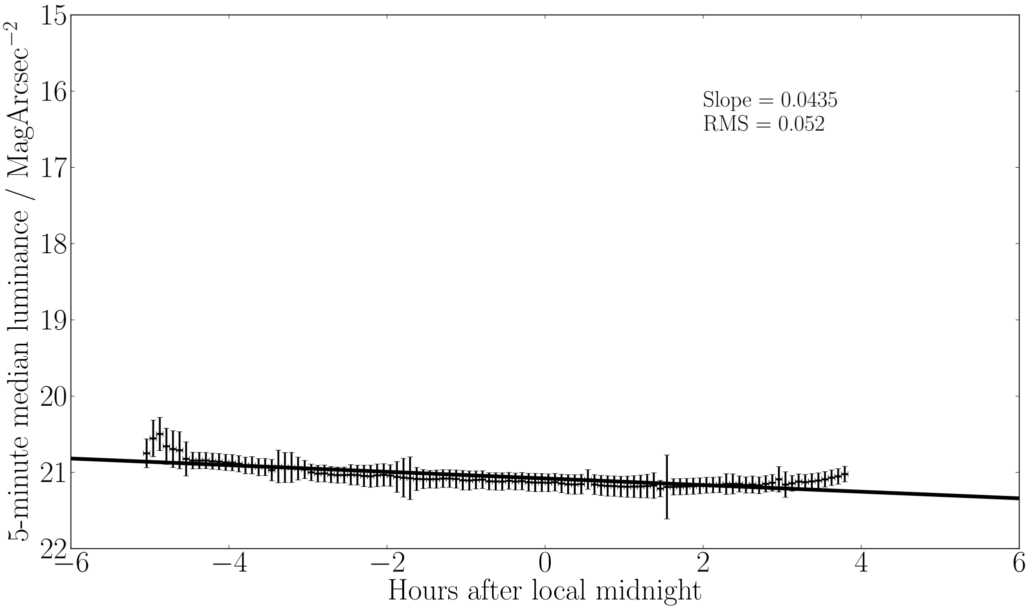

Average cloud-free night sky luminance time series

RadioKootwijk (Site ID: 19)

Cloud Coverage Analysis

Oktas	Data count	Median luminance	Uncertainty			
			Instrumental	1-minute geophysical	Subset geophysical	Total
0	120	20.721	0.101	0.008	0.060	0.118
1	150	20.787	0.101	0.005	0.028	0.105
2	30	20.693	0.101	0.006	0.026	0.104
4	37	20.773	0.101	0.030	0.065	0.124
6	30	20.608	0.101	0.008	0.115	0.154
7	30	20.412	0.101	0.013	0.053	0.115
8	283	20.397	0.101	0.030	0.699	0.707

Cloud Amplification Factor

Oktas	Amplification factor
1	0.941 ± 0.865
2	1.026 ± 0.865
4	0.953 ± 0.854
6	1.110 ± 0.837
7	1.329 ± 0.859
8	1.348 ± 0.517

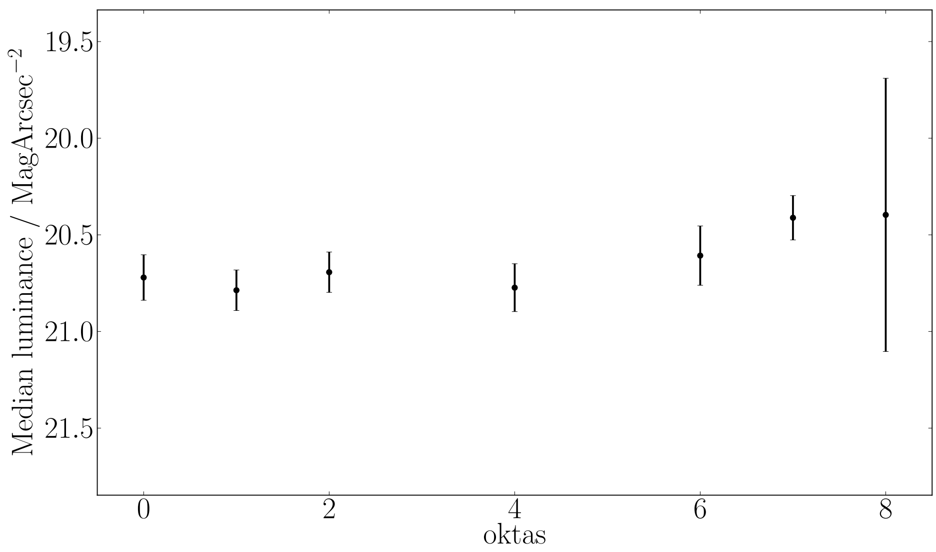

Cloud coverage analysis plot

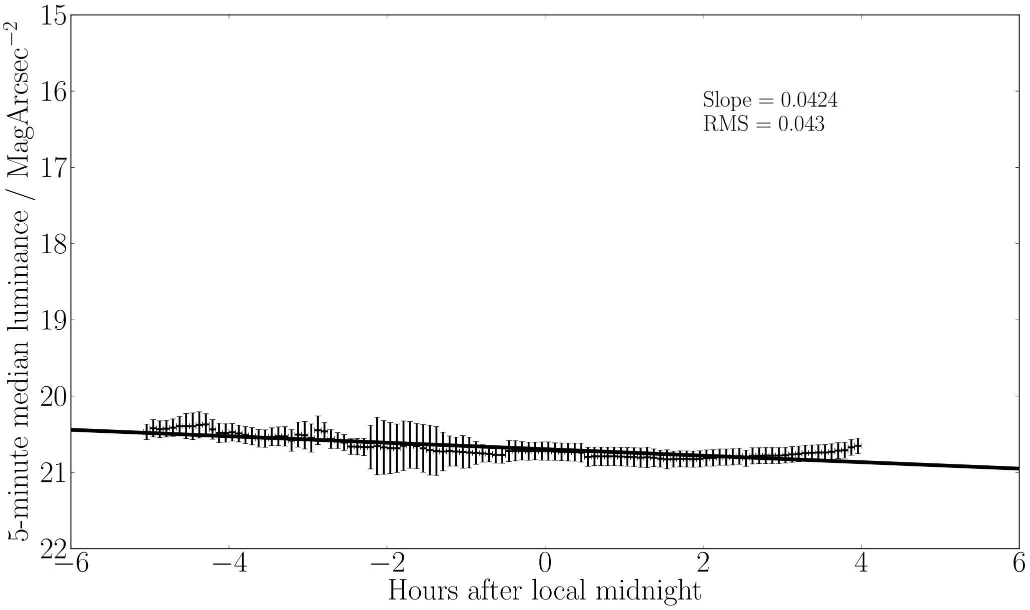

Average cloud-free night sky luminance time series

Schiermonnikoog (Site ID: 20)

Cloud Coverage Analysis

Oktas	Data count	Median luminance	Uncertainty			
			Instrumental	1-minute geophysical	Subset geophysical	Total
0	149	20.678	0.101	0.012	0.224	0.246
1	30	21.448	0.101	0.003	0.003	0.101
2	60	20.959	0.101	0.022	0.524	0.534
3	30	21.337	0.101	0.005	0.010	0.102
4	30	20.299	0.101	0.032	0.107	0.150
7	90	20.658	0.101	0.013	0.341	0.356
8	120	21.474	0.101	0.013	0.522	0.531

Cloud Amplification Factor

Oktas	Amplification factor
1	0.492 ± 0.782
2	0.772 ± 0.582
3	0.545 ± 0.782
4	1.418 ± 0.766
7	1.018 ± 0.671
8	0.480 ± 0.583

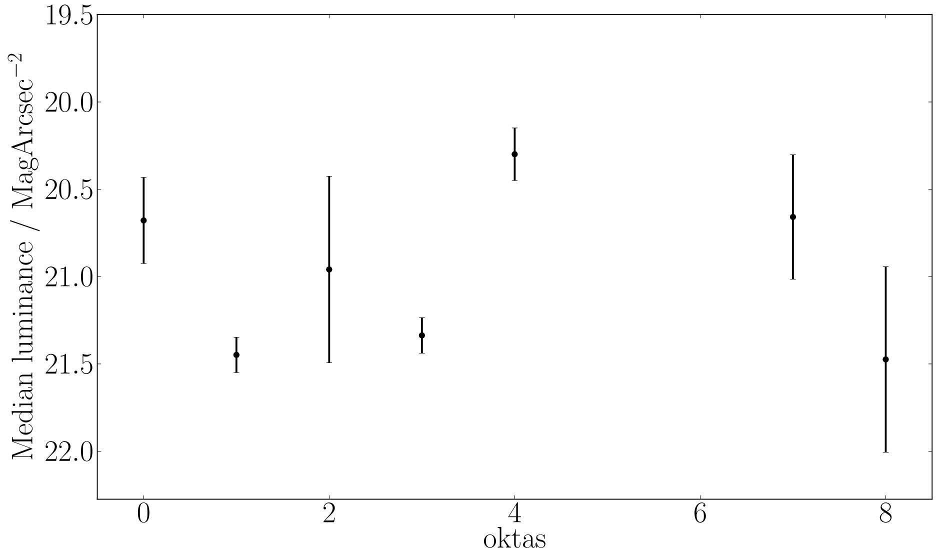

Cloud coverage analysis plot

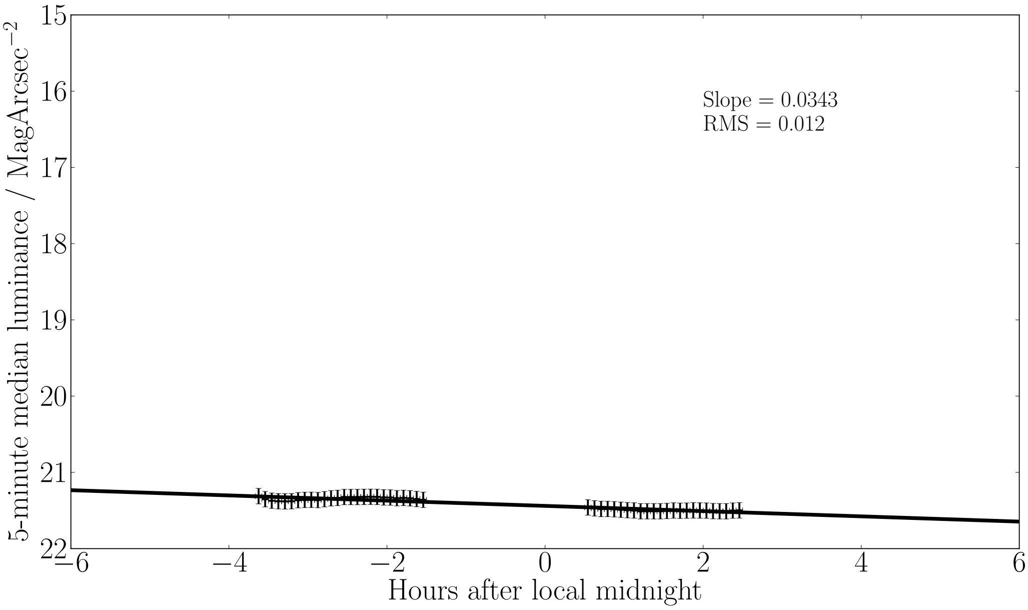

Average cloud-free night sky luminance time series

Schipluiden (Site ID: 21)

Cloud Coverage Analysis

Oktas	Data count	Median luminance	Uncertainty			
			Instrumental	1-minute geophysical	Subset geophysical	Total
0	494	18.614	0.109	0.035	0.480	0.494
1	90	18.438	0.106	0.052	0.229	0.258
2	60	17.937	0.124	0.198	0.371	0.438
3	30	18.451	0.105	0.023	0.012	0.108
4	60	18.123	0.235	0.209	1.342	1.378
6	90	16.697	0.223	0.198	0.897	0.945
8	661	16.067	0.303	0.126	1.063	1.113

Cloud Amplification Factor

Oktas	Amplification factor
1	1.177 ± 0.598
2	1.866 ± 0.544
3	1.163 ± 0.628
4	1.572 ± 0.260
6	5.845 ± 0.374
8	10.449 ± 0.326

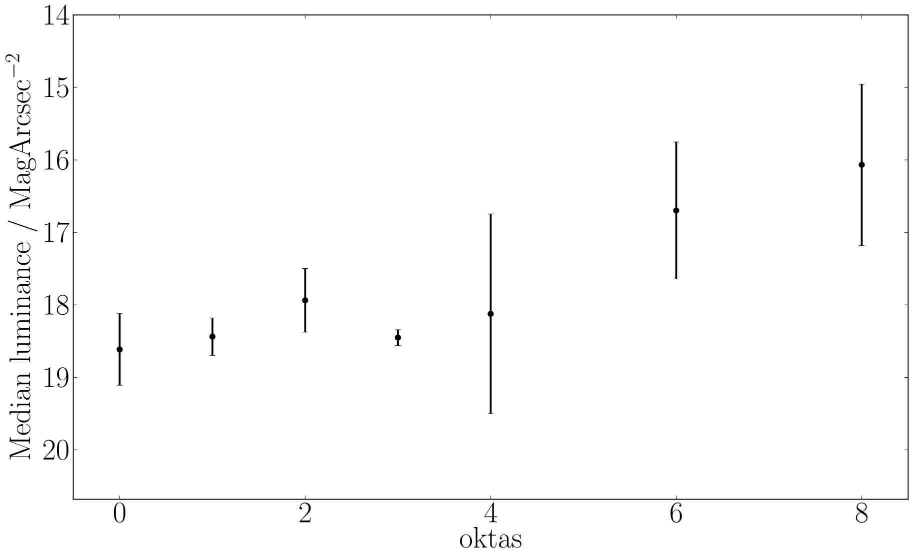

Cloud coverage analysis plot

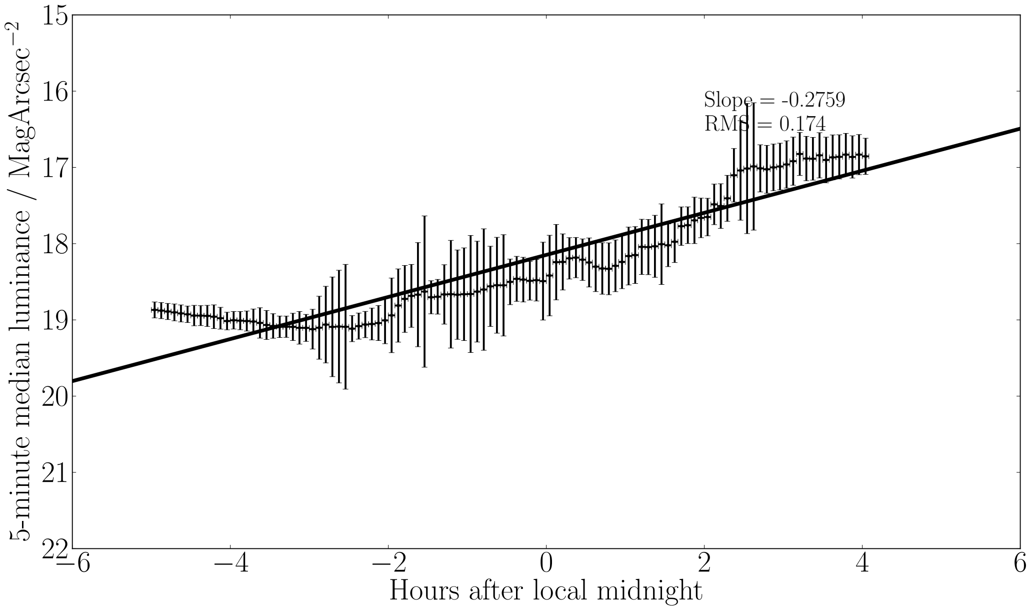

Average cloud-free night sky luminance time series

trueblood (Site ID: 22)

Cloud coverage analysis and cloud amplification factor: No data

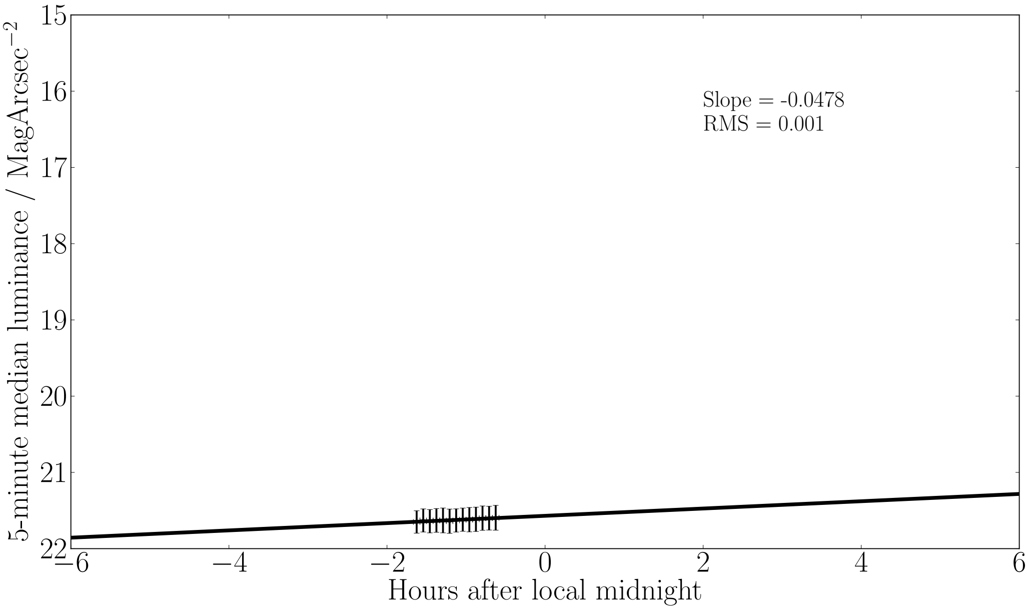

Average cloud-free night sky luminance time series

unihedron (Site ID: 23)

Cloud coverage analysis and cloud amplification factor: No data

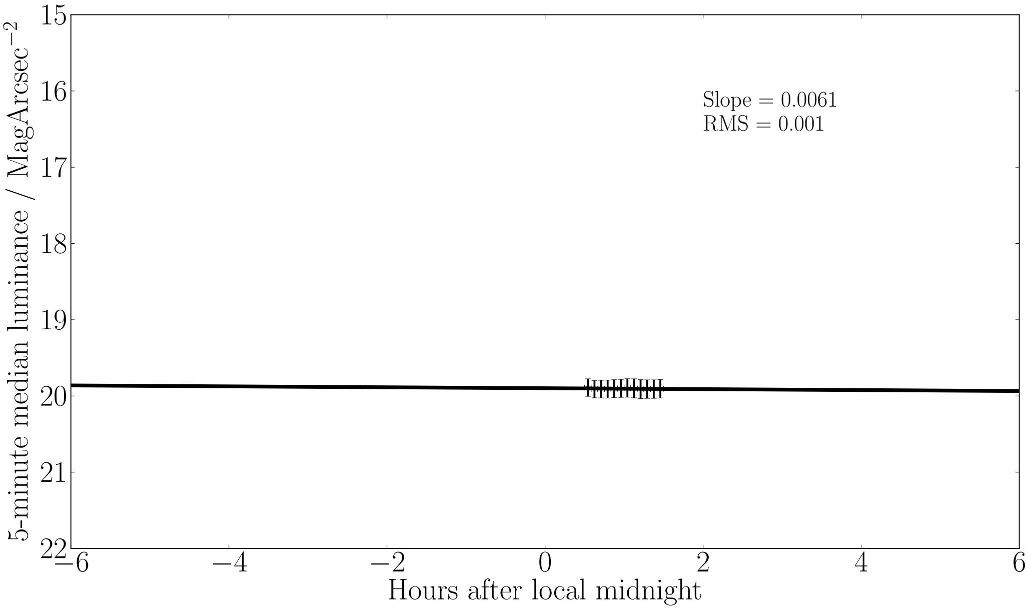

Average cloud-free night sky luminance time series

Utrecht (Site ID: 24)

Cloud Coverage Analysis

Oktas	Data count	Median luminance	Uncertainty: Instrumental	Uncertainty: 1-minute geophysical	Uncertainty: Subset geophysical	Uncertainty: Total
0	20	18.970	0.101	0.000	0.068	0.122
1	30	18.775	0.114	0.000	0.616	0.626
4	20	18.625	0.108	0.000	0.517	0.528
7	12	17.740	0.173	0.000	1.018	1.033
8	30	16.290	0.224	0.000	0.938	0.964

Cloud Amplification Factor

Oktas	Amplification factor
1	1.197 ± 0.556
4	1.374 ± 0.607
7	3.105 ± 0.384
8	11.803 ± 0.409

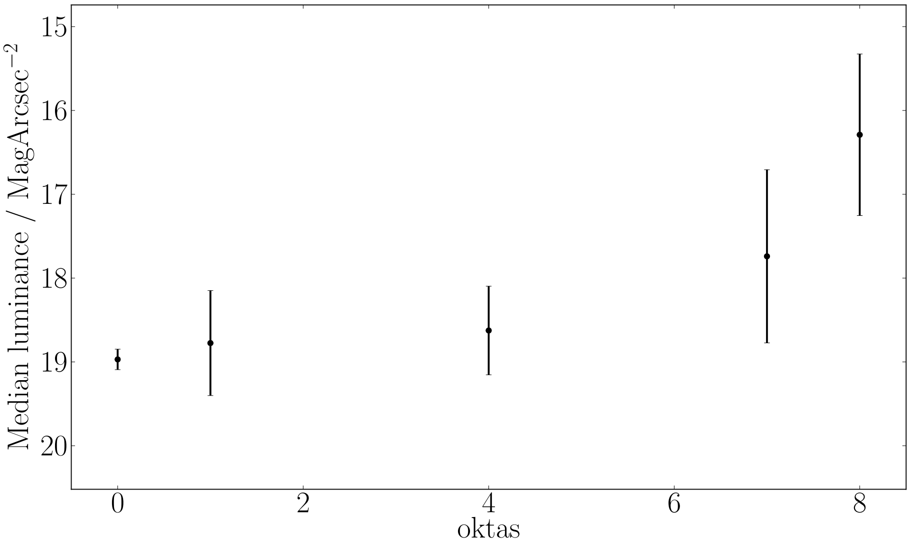

Cloud coverage analysis plot

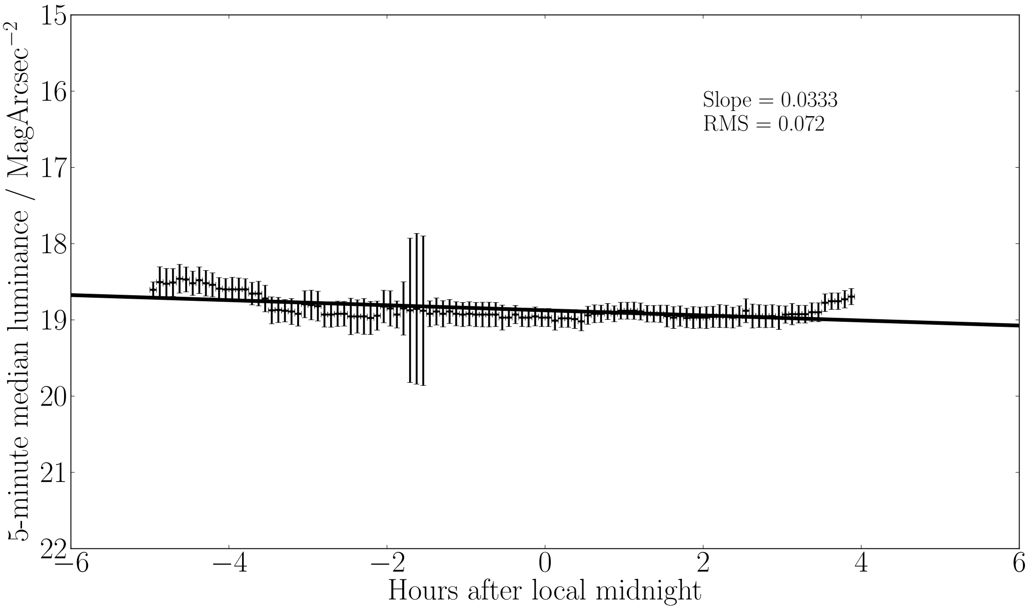

Average cloud-free night sky luminance time series

Vlaardingen (Site ID: 26)

Cloud Coverage Analysis

Oktas	Data count	Median luminance	Uncertainty			
			Instrumental	1-minute geophysical	Subset geophysical	Total
0	495	17.356	0.144	0.045	0.217	0.264
1	90	17.241	0.154	0.074	0.563	0.588
2	60	17.337	0.147	0.151	0.327	0.389
3	30	17.275	0.152	0.041	0.124	0.200
4	60	17.032	0.237	0.082	0.783	0.822
6	60	16.568	0.235	0.110	0.420	0.494
8	603	16.040	0.268	0.076	0.651	0.708

Cloud Amplification Factor

Oktas	Amplification factor
1	1.111 ± 0.552
2	1.017 ± 0.648
3	1.077 ± 0.737
4	1.348 ± 0.451
6	2.065 ± 0.597
8	3.360 ± 0.498

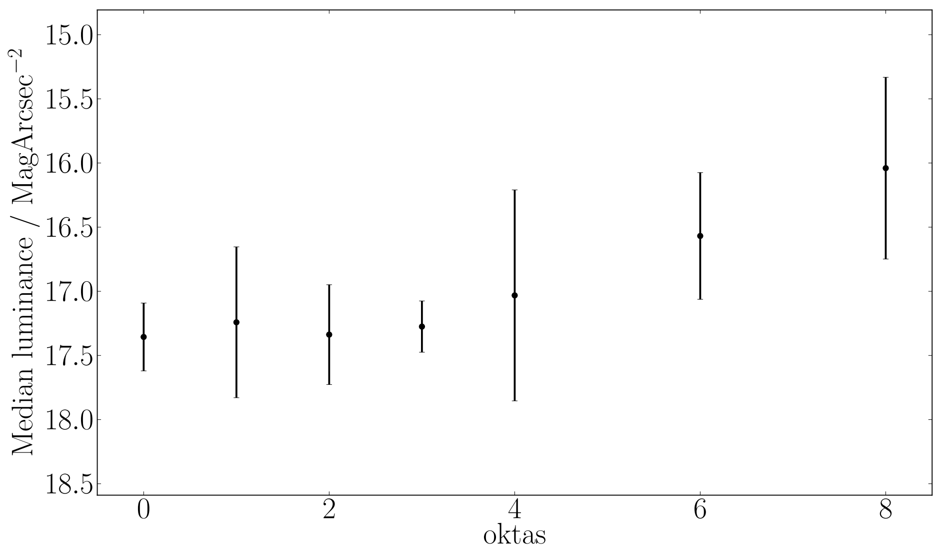

Cloud coverage analysis plot

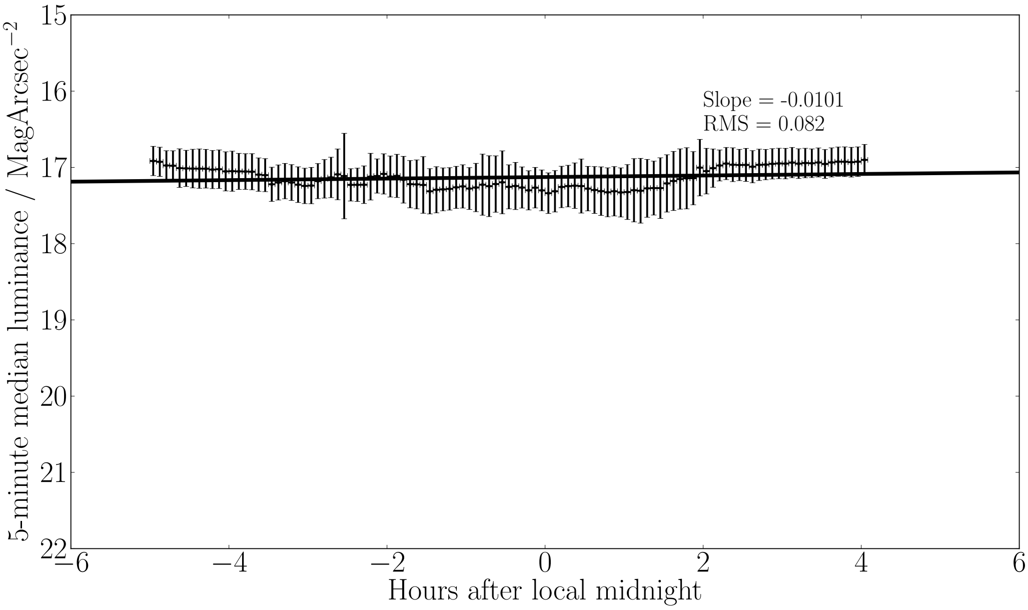

Average cloud-free night sky luminance time series

Appendix B

List of Data Providers of International SQM Survey

Site ID(s)	Name of contact person / organization
3, 13, 17, 19, 20, 21, 24, 26	RIVM (National Institute for Public Health and the Environment), The Netherlands
8, 9, 10, 11, 12	BuioMetria Partecipativa, Italy
15	John Kuehn, DeerLick Astronomy Village, USA
6	Dr. Chrisopher C. M. Kyba , Institute for Space Sciences, Freie Universität Berlin, Germany
7	Robert Schwarz , Leibniz-Institut für Astrophysik Potsdam, Germany
23	Anthony Tekatch, Unihedron, Canada
22	Mark Trueblood, Winer's Observatory, USA
16	Prof. Douglas L. Welch, Department of Physics and Astronomy, McMaster University, Canada

Bibliography

[1] R. L. Berry. Light pollution in Southern Ontario. *Journal of the Royal Astronomical Society of Canada*, 70:97–115, June 1976.

[2] P. Cinzano. Night sky photometry with sky quality meter. ISTIL Internal Report n. 9, v 1.4, ISTIL, Thiene, 2005.

[3] P. Cinzano, F. Falchi, and C. D. Elvidge. The first world atlas of the artificial night sky brightness. *Monthly Notices of the Royal Astronomical Society*, 328(3):689–707, 2001.

[4] Commission Internationale de l´Eclairage. Photometry - The CIE System of Physical Photometry. ISO 23539: 2005(E) / CIE S 010/E: 2004, 2005.

[5] R. H. Garstang. Night-sky brightness at observatories and sites. *Publications of the Astronomical Society of the Pacific*, 101:306–329, March 1989.

[6] F. Giubbilini and A. Giacomelli. Sky Quality Meter cross-calibration in the BMP project. Working paper, BuioMetria Partecipativa, Italy, March 2011.

[7] A. Hänel. The increase in light pollution in central Europe. In *Proceedings of the Dark-Skies Symposium*, Portsmouth, UK, 2006.

[8] C. S. Holt and T. F. Waters. Effect of light intensity on the drift of stream invertebrates. *Ecology*, 48(2):225–234, 1967.

[9] S. R. James, R. W. Dennell, A. S. Gilbert, H. T. Lewis, J. A. J. Gowlett, T. F. Lynch, W. C. McGrew, C. R. Peters, G. G. Pope, A. B. Stahl, and S. R. James. Hominid use of fire in the lower and middle pleistocene: A review of the evidence [and comments and replies]. *Current Anthropology*, 30(1):1–26, 1989.

[10] H. L. Johnson and W. W. Morgan. Fundamental stellar photometry for standards of spectral type on the revised system of the Yerkes spectral atlas. *Astrophysical Journal*, 117:313–352, May 1953.

[11] D. W. Johnston and T. P. Haines. Analysis of Mass Bird Mortality in October, 1954. *The Auk*, 74(4):447–458, 1957.

[12] C. C. M. Kyba, T. Ruhtz, J. Fischer, and F. Hölker. Cloud coverage acts as an amplifier for ecological light pollution in urban ecosystems. *PLoS ONE*, 6(3):e17307, March 2011.

[13] C. C. M. Kyba, T. Ruhtz, J. Fischer, and F. Hölker. Red is the new black: how the colour of urban skyglow varies with cloud cover. *Monthly Notices of the Royal Astronomical Society*, 2012.

[14] C. Leinert, S. Bowyer, L. Haikala, M. Hanner, M. Hauser, A.-C. Levasseur-Regourd, I. Mann, K. Mattila, W. Reach, W. Schlosser, H. Staude, G. Toller, J. Weiland, J. Weinberg, and A. Witt. The 1997 reference of diffuse night sky brightness. *Astronomy and Astrophysics Supplement Series*, 127(1):1–99, 1998.

[15] H. Letu, G. Tana, M. Hara, and F. Nishio. Monitoring the electric power consumption by lighting from DMSP/OLS nighttime satellite imagery. In *Geoscience and Remote Sensing Symposium (IGARSS), 2011 IEEE International*, pages 2113 –2116, July 2011.

[16] Q. Li, T. Zheng, T. R. Holford, P. Boyle, Y. Zhang, and M. Dai. Light at night and breast cancer risk: results from a population-based case-control study in Connecticut, USA. *Cancer Causes & Control*, 21(12):2281–2285, 2010.

[17] Z. Liu, C. He, and Y. Yang. Mapping urban areas by performing systematic correction for dmsp/ols nighttime lights time series in china from 1992 to 2008. In *Geoscience and Remote Sensing Symposium (IGARSS), 2011 IEEE International*, pages 1858 –1861, July 2011.

[18] T. Longcore and C. Rich. Ecological light pollution. *Frontiers in Ecology and the Environment*, 2(4):191–198, 2004.

[19] D. McKenna. Status of the Vatican Observatory/IDA Night Sky Brightness Monitor (NSBM). Project report, International Dark-Sky Association, USA, October 2008.

[20] E. F. F. Milone and C. Sterken. *Astronomical photometry: past, present, and future*. Astrophysics and space science library ; 373. Springer, New York, NY, 2011. XII, 217 S.

[21] K. J. Navara and R. J. Nelson. The dark side of light at night: physiological, epidemiological, and ecological consequences. *Journal of Pineal Research*, 43(3):215–224, 2007.

[22] K. W. Riegel. Light pollution. *Science*, 179(4080):1285–1291, 1973.

[23] W. Rowan. Relation of light to bird migration and developmental changes. *Nature*, 115:494–495, 1925.

[24] R. Salgado-Delgado, A. T. Osorio, N. Saderi, and C. Escobar. Disruption of circadian rhythms: A crucial factor in the etiology of depression. *Depression Research and Treatment*, 2011, 2011.

[25] C. W. So. Observational studies of the night sky in Hong Kong. Master of philosophy thesis, The University of Hong Kong, Hong Kong, 2010.

[26] C. W. So and J. C. S. Pun. Report of a survey of light pollution in Hong Kong. Project report, The University of Hong Kong, Hong Kong, 2010.

[27] H. Stark, S. S. Brown, W. P. Dube, N. Wagner, T. B. Ryerson, I. B. Pollack, and D. D. Parrish. Nighttime photochemistry: nitrate radical destruction by anthropogenic light sources. *AGU Fall Meeting Abstracts*, page C117, Dec. 2010.

[28] Statistisches Landesamt Bremen. Statistisches Jahrbuch 2011. Bremen, 2011.

[29] C. Sterken and J. Manfroid. *Astronomical photometry : a guide*. Kluwer Academic Publishers, Dordrecht Boston, 1992.

[30] R. G. Stevens. Light-at-night, circadian disruption and breast cancer: assessment of existing evidence. *International Journal of Epidemiology*, 38(4):963–970, 2009.

[31] S. Twomey, R. Gall, and M. Leuthold. Pollution and cloud reflectance. *Boundary-Layer Meteorology*, 41:335–348, 1987.

[32] C. Vollmer, U. Michel, and C. Randler. Outdoor light at night (LAN) is correlated with eveningness in adolescents. *Chronobiology International*, 29(4):502–508, 2012.

[33] M. F. Walker. The effects of urban lighting on the brightness of the night sky. *Astronomical Society of the Pacific, Publications*, 89:405–409, June 1977.

[34] A. Weigert, H. J. Wendker, and L. Wisotzki. *Astronomie und Astrophysik : Ein Grundkurs*. Wiley-VCH, Weinheim, Bergstr, 2009.

[35] World Metreological Organization. FM system of numbering code forms. *Manual of Codes, WMO No. 306*, I.1:A.1 – A.71, 2009.